sciendo
Austrian Journal of Earth Sciences | Vienna | 2022 | Volume 115 | 41 - 73 | DOI: 10.17738/ajes.2022.0003

From shallow into deep sea: Sedimentary facies and U-Pb zircon ages in the early Paleozoic Noric Group at Veitsch (Eastern Greywacke Zone, Austria)

Josef Nievoll[1], Harald Fritz[2*], Daniela Gallhofer[2], Christoph Hauzenberger[2], Michael Pfatschbacher[2,3], Bernadette Gritsch[2,4]

[1] Gumpendorfer Straße 83–85/2/48, 1060 Wien, Austria; josef.nievoll@gmail.com.

[2] NAWI Graz Geocenter – University of Graz. Institute of Earth Sciences, Universitätsplatz 2, Graz 8010. Austria; harald.fritz@uni-graz.at; daniela.gallhofer@uni-graz.at; christoph.hauzenberger@uni-graz.at.

[3] Hasel 21, 8795 Radmer; michael.pfatschbacher@hotmail.com.

[4] Mühldorfergasse 26A, 5020 Salzburg; bernadette-g@gmx.at.

[*] Corresponding author, Harald Fritz; harald.fritz@uni-graz.at

KEYWORDS

Eastern Alps, Eastern Greywacke Zone; U/Pb zircon data, sedimentary facies, tectonics.

Abstract

The low-grade metamorphic early Paleozoic basement of the Veitsch area presents a wide variety of sedimentary facies domains. The first domain consists of thick metadacites of Middle Ordovician age (Blasseneck Porphyroid), overlain by fine-grained metaclastics of the Rad Formation (Late Ordovician to Silurian) and Devonian limestones and calcitic marbles (Kaiserstein and Kaskögerl Formation, respectively). Rhyolitic to dacitic magmatism initiated at ca. 479 Ma (LA-MC-ICP-MS U-Pb zircon data) and lasted until ca. 444 Ma. The second domain comprises metaclastics of the Stocker Formation (Early Ordovician to Silurian), characterized by thin volcanics and volcaniclastics of andesitic and rhyolitic composition. U-Pb zircon data give Middle Ordovician age (463 Ma – 468 Ma). The third domain, exposed northwest of Veitsch, consists of thick metadacites (Blasseneck Porphyroid, ca. 478 Ma), followed by (siliceous) phyllites which grade into turbiditic metasediments (Sommerauer Formation, Late Ordovician to Devonian?). Clastic sediments of the Stocker and Sommerauer Formations were sourced from northern Gondwana showing a prominent Pan-African detrital zircon peak at ca. 640 Ma. Middle to Upper Ordovician volcanics (ca. 462 Ma – 448 Ma) represent the second source. Tectonic reconstruction leads us to the arrangement of three facies domains. A shallow marine shelf facies is located in the present days southwest. A marginal basin with volcanic islands on a sloping continent, and a deep-water environment containing turbidites are situated further to the northwest. The present arrangement of these facies domains is explained by eo-Alpine and Variscan thrust tectonics.

Kurzfassung

Der niedrig metamorphe altpaläozoische Sockel der Norischen Decke in der Umgebung von Veitsch umfasst verschiedene sedimentäre Fazieszonen. Der erste Faziesbereich umfasst den mächtigen, vorwiegend mittelordovizischen Blasseneck-Porphyroid, der von feinkörnigen Metaklastika der Rad-Formation (oberes Ordoviz bis Silur) und Kalkmarmoren der Kaiserstein- und Kaskögerl-Formation (Devon) überlagert wird. Der rhyolitische und dazitische Magmatismus begann vor ca. 479 Ma (LA-MC-ICP-MS U-Pb Zirkonalter) und dauerte bis etwa 444 Ma. Der zweite Faziesbereich umfasst die Stocker-Formation (unteres Ordoviz bis Silur), die geringmächtige Vulkanite andesitischer und rhyolitischer Zusammensetzung enthält (mittleres Ordoviz, 463 Ma – 468 Ma), sowie Kalkmarmore der Kaskögerl-Formation (Devon). Im dritten Faziesbereich, der in der Umgebung von Aschbach nordwestlich von Veitsch auftritt, wird der mächtige unterordovizische Blasseneck-Porphyroid (ca. 478 Ma) von Metaklastika der Sommerauer-Formation überlagert, die Charakteristika von Turbiditen aufweisen (oberes Ordoviz bis möglicherweise Devon). Das Liefergebiet der klastischen Sedimente der Stocker- und Sommerauer-Formation war der nördliche Rand Gondwanas, belegt durch eine ausgeprägte Häufung panafrikanischer detritischer Zirkone bei etwa 640 Ma. Ein zweites Liefergebiet stellen mittel- bis oberordovizische Vulkanite dar (ca. 462 Ma – 448 Ma). Die Abwicklung der Tektonik ergibt die heutige räumliche Anordnung der Faziesräume mit einer flachmarinen Fazies im Südwesten, gefolgt von einem Randbecken mit vulkanischen Inseln. Tiefwassersedimente mit Turbiditen am Fuß des Kontinentalhanges schließen nach Nordwest an. Die heutige Anordnung dieser Faziesbereiche wird durch variszische und altalpidische Deckentektonik erklärt.

1. Introduction

The term "Grauwackenzone", i.e. "Greywacke Zone", was originally introduced to describe the hilly domain between the Northern Calcareous Alps and the "crystalline" rocks of the central axis of the Alps (Hauer, 1868; Stur, 1871). After 150 years of geologic investigations, this term is still widely used for denoting the low-grade metamorphic, fossiliferous Paleozoic basement of the Northern Calcareous Alps, although Schuster (2015) in his review considered it as a geographic unit. Geologically, it turned out to be much more complex than just formed by "transitional rocks" as envisaged during the heroic times of the k.k. Geologische Reichsanstalt. In the western part, rocks of the Greywacke Zone form the early Paleozoic basement of the Tirolic nappes of the Northern Calcareous Alps. In the eastern part, the Noric Thrust was introduced (Metz, 1938; Cornelius, 1952) to highlight the tectonic contact between a lower Veitsch Nappe, a sequence of Carboniferous shallow marine molasse sediments, and a higher Noric Nappe (Cornelius, 1952), made up of early Paleozoic rocks upon which, like in the western part, Tirolic units of the Northern Calcareous Alps are transgressing. More detailed mapping in the Veitsch area revealed that the Noric Thrust in fact is an anastomosing thrust system; one of the thrusts is running at the base of the Blasseneck Porphyroid and is marked by slices of magnesite, amphibolite and gneiss (Nievoll, 1984). The revised and widely accepted tectonostratigraphy of the Eastern Greywacke Zone (Neubauer et al., 1994; Schuster, 2015; Haas et al., 2020) includes from tectonic bottom to top, (1) the Veitsch Nappe (Ratschbacher, 1984; Neubauer and Vozarova, 1990); (2) the Silbersberg Nappe, representing a succession of Permian metaclastics interbedded with acidic and basic volcanics, and (3) slices of amphibolite and gneiss ("Kaintaleck slices") of debated tectonic position (Kaintaleck Nappe; Neubauer et al., 1994; 2002 or part of the Silbersberg Nappe; Schuster, 2015). (4) The top part of the Greywacke Zone is represented by early Paleozoic metasediments and metavolcanics transgressively overlain by Permo-Mesozoic sediments in Tirolic facies. Consequently, the Noric Nappe (Cornelius, 1952) and its Permo-Mesozoic cover constitute together the Tirolic-Noric Nappe System (Schuster, 2015). The Tirolic-Noric Nappe System itself is topped by the Juvavic Nappe System, represented in the study area by the Mürzalpen Nappe, which consists of Permian evaporitic sediments (Haselgebirge), a few displaced Permian gabbros (Mandl, 2015) and Triassic limestones in Hallstatt facies (Fig. 1).

To distinguish between lithostratigraphic and tectonic terms, we use „Noric Group" (Neubauer et al., 1994) for the formations described in chapter 3 (Lithostratigraphy and sedimentary facies of the Noric Group) and Noric Nappe (Cornelius, 1952) for the set of internal nappes described in chapter 5 (Tectonic structure of the Noric Nappe). In the present paper we describe U-Pb zircon age data from metavolcanics and metasandstones, the sedimentary facies of the individual formations and the tectonic structure of the Noric Nappe between Stübming in the west and Neuberg in the east (Fig. 2). A full-scale version of the geological map including topographic information is provided in the supplementary material as Figure S1. Retro-deformation of the tectonic structure results in an arrangement of facies domains between early Ordovician and Devonian times ranging from shallow water into deep sea. Our facies model is compared with other well-studied areas of the Greywacke Zone, like the Eisenerz Mountains in the Eastern Greywacke Zone (Schönlaub, 1982; Bryda et al., 2013) and the Kitzbühel area in the Western Greywacke Zone (Heinisch et al., 2015).

2. Geological Setting

The Eisenerz Mountains, located approx. 50 km west of Veitsch, were traditionally the preferred region to unravel the stratigraphy of the Eastern Greywacke Zone. In the second half of the 19th century macrofossils had been discovered at several locations during iron ore mining and exploring (Schouppe, 1854; Stur, 1865). A major breakthrough was achieved from 1963 onwards by detailed sampling of limestones for conodonts (see review in Schönlaub, 1982). The age of the Blasseneck Porphyroid, one of the marker beds of the entire Greywacke Zone, was determined as Late Ordovician (Flajs and Schönlaub, 1976). With the conodont data, several new formations were introduced and attributed to facies realms, now distributed within distinct internal nappes (Zeiritzkampl-, Wildfeld-, Reiting-Nappes, Schuppenzone and Nordzone). The stratigraphic succession, although not continuous, ranges from Early to Middle Ordovician to Middle Mississippian (Visean) with Carboniferous conodonts preserved only locally in limestone breccias filling a paleo-relief. Metaclastics of probably Late Visean to Early Pennsylvanian age (Eisenerz Formation; Schönlaub et al., 1980) are the youngest sediments affected by Variscan tectonics. Conglomerates and sandstones of the Permian Präbichl Formation are sealing the Variscan nappe structures (Neubauer, 1989).

The Noric Group in the study area differs in important aspects from the formations of the Eisenerz Mountains. Macrofossils have been discovered much later (Nievoll, 1983), conodonts are less frequent and more recrystallized (Ebner, 1974; Nievoll; 1987), and prominent formations exposed in the Eisenerz area like Gerichtsgraben Formation, Polster Quartzite, Ordovician and Silurian marbles, basic volcanics and Eisenerz Formation are absent or occurring only locally with strongly reduced thickness. Therefore, a new set of formations has been described (Nievoll and Suttner, 2015) which comprise from bottom to top (1) Blasseneck Porphyroid of predominantly dacitic composition, (2) the Rad Formation, uniform fine-grained metasediments, locally containing macrofossils of Late Ordovician to Silurian age, (3) Devonian limestone marbles and calcareous phyllites (Kaiserstein and Kaskögerl Formations), and (4) the Stocker Formation, consisting of phyllites with thin layers of intermediate and acidic volcanics, volcaniclastics, sandstones, quartzites and

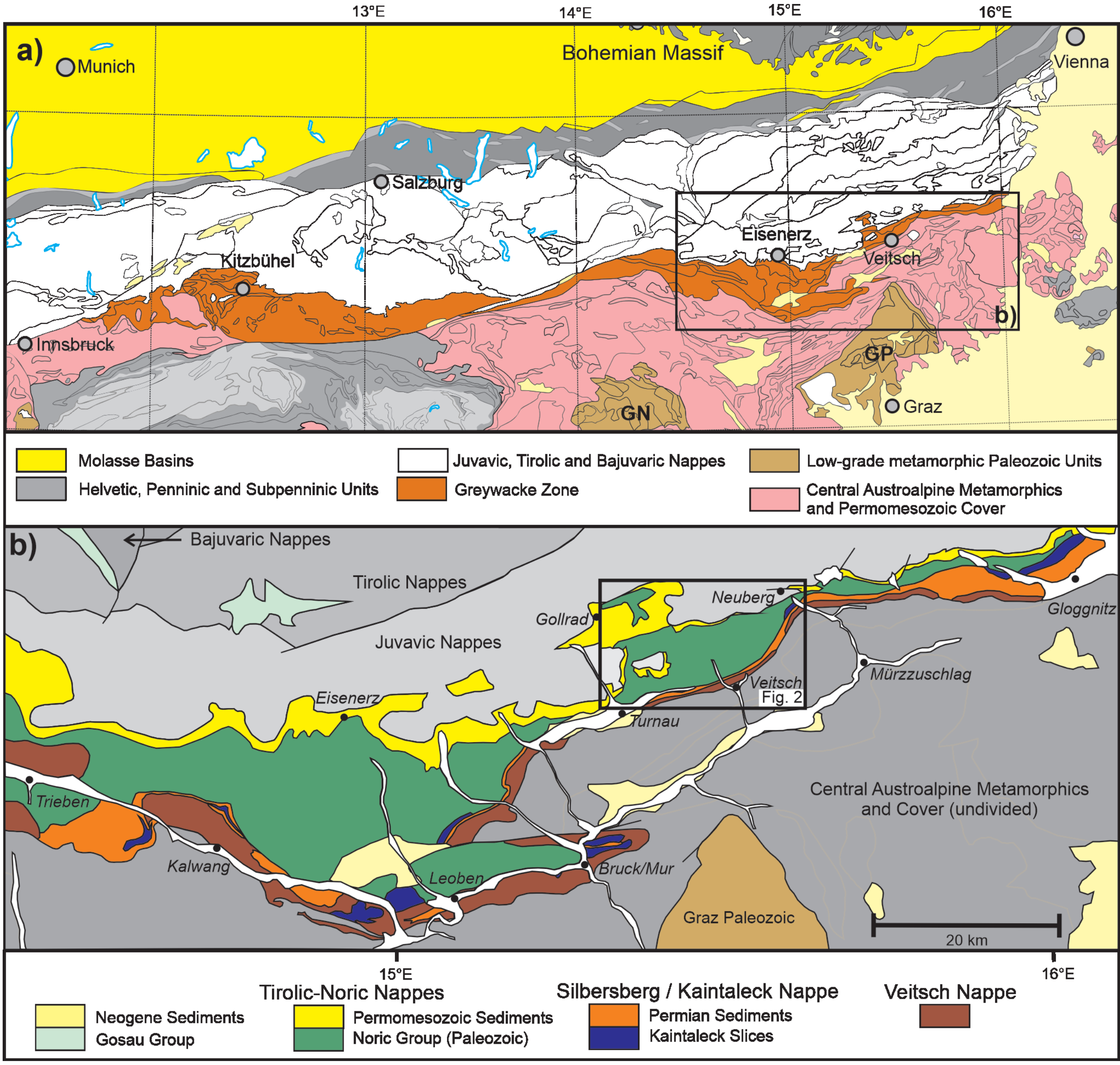

Figure 1: (a) Simplified map of the northern sector of the Eastern Alps (GP: Graz Paleozoic; GN: Gurktal Nappe System). Frame delineates the eastern part of the Eastern Greywacke Zone. **(b)** Map of the Eastern Greywacke Zone and adjacent units redrawn from maps provided by the Austrian Geological Survey (https://www.geologie.ac.at/). Frame shows the study area (Fig. 2).

siliceous phyllites of uncertain age. The nappe structure in the study is resolved from repetition of characteristic lithologies. Based upon this, four Tirolic-Noric nappes (Hocheck, Rossegg, Steinbach and Aschbach nappes) and one Juvavic nappe (Rauschkogel klippe, part of the Mürzalpen Nappe) are distinguished (full details are given in chapter 5).

The Blasseneck Porphyroid occupies about two thirds of the outcropping Noric Nappe. Over most of the study area it is sheared off along the Noric Thrust and rests upon the Silbersberg Nappe or tectonic slices of magnesite (Veitsch Nappe), amphibolite or gneiss (Nievoll, 1984) (Fig. 2). Immediately above the Noric Thrust the Blasseneck Porphyroid has a mylonitic fabric and dips steeply to the north and northwest. Quartz phenocrysts are, however, preserved even in mylonitic Blasseneck Porphyroid and allow an unequivocal distinction from Silbersberg phyllites. Metaclastics and thin calcitic marbles beneath the Blasseneck Porphyroid which are attributed to the Gerichtsgraben Formation occur only in the very southwest of the study area. Between Veitsch and Neuberg the formations in the hangingwall of the Blasseneck Porphyroid are dipping steeply to the northwest. Rad and Stocker Formations are best preserved between upstream sections of Groß- and Kleinveitsch valleys; from Kleinveitsch towards northeast all formations above the Blasseneck Porphyroid are progressively thinning out.

Towards the west, the entire Noric Nappe is cut by a major northwest trending tear fault (Almweg Fault; Nievoll, 2015)

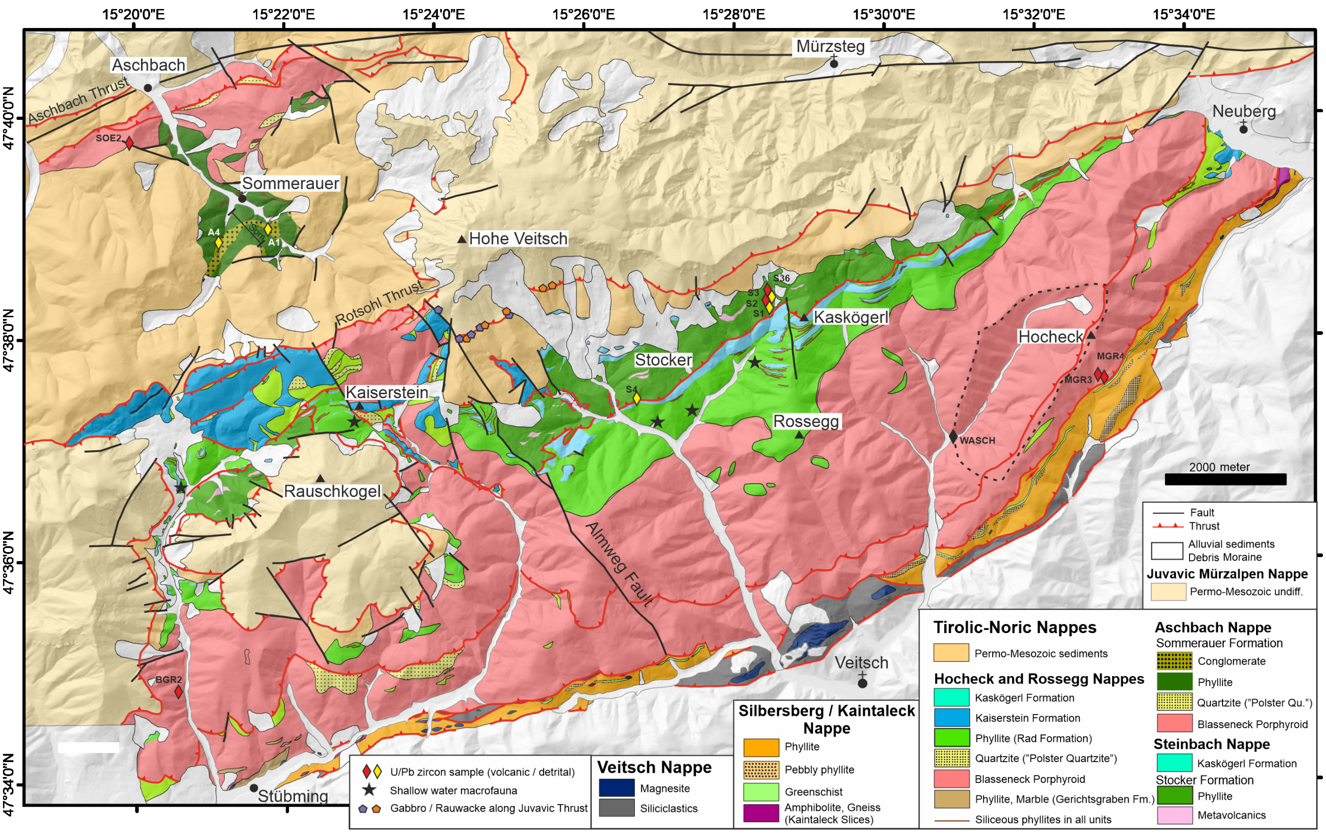

Figure 2: Simplified geological map of the Eastern Greywacke Zone between Aschbach and Stübming in the West and Neuberg in the East. Sample sites for fossils and U/Pb zircon analyses, as well as significant lithologies (gabbro, rauwacke) defining the base of Juvavic Mürzalpen Nappe are indicated. Name-giving sites for formations (Stocker, Sommerauer) and nappes (Hocheck, Rossegg, Steinbach, Aschbach) are given. The abbreviation Som (Sommerauer) gives site of detail section of the Sommerauer Formation (Fig. 8b). Note that U/Pb zircon sample WASCH (black diamond) derived from river sands of the Taurisgraben. Catchment area of this sample is indicated by the stippled line adjacent to WASCH. A full-scale version of the geological map including topographic information is provided in the supplementary material as Figure S1.

(Figs 2-3). West of this fault, the Blasseneck Porphyroid and the Kaiserstein Formation are dipping generally gently to the south. Displacement along the Almweg Fault is not merely vertical as interpreted previously (Cornelius; 1939, 1952) but rather horizontal, accommodating different amounts of thrust-related displacement on both sides (Haller, 2016). The Blasseneck Porphyroid and the calcitic marbles of the Kaiserstein Formation to the west of this fault display fold- and thrust structures formed above a ramp that overthrusted and inverted the Permian Präbichl Formation along the Rotsohl Thrust (Fig. 4). This ramp structure is responsible for the great thickness of the Präbichl and Werfen Formations south of Aschbach which was already noted in the 19th century (Stur, 1871); it explains also the abrupt western end of the Juvavic Mürzalpen Nappe of Hohe Veitsch (Figs 2-3).

A similar structure including ramp antiforms and imbricate thrust splays is exposed 4.5 km to the northwest in Aschbach where the Blasseneck Porphyroid is thrust upon the Präbichl Formation (Aschbach Thrust: Fig. 4) or dipping steeply beneath it (Niederalpl). Here, on top of the Blasseneck Porphyroid metaclastics crop out in the Rotsohl valley which are described in more detail in chapter 3.4.

In the southwest of the study area, the Noric Nappe is topped by the Rauschkogel klippe pertaining to the Mürzalpen Nappe (Mandl, 2015). Further to the west, the Noric Nappe is buried beneath the Mürzalpen Nappe of Hochanger and Osterer Alm and the Miocene sediments of the Aflenz basin (not shown on the map), respectively.

The study area presents a typical "Greywacke Zone morphology", with altitudes between 700 and 1400 m above sea-level, covered almost entirely by forests; outcrops are limited to creeks and forest roads. The rocks have suffered low-grade metamorphism during Variscan and eo-Alpine (Cretaceous) times, the latter having been investigated by numerous authors (e.g., Ratschbacher, 1984; Neubauer et al., 1994; Dallmeyer et al., 1996, 1998; Schuster and Frank, 1999; Frank and Schlager, 2006; Rantitsch et al., 2020). Variscan metamorphism is documented by metamorphic clasts of the Präbichl Formation derived from the Noric Nappe (Cornelius, 1952). The eo-Alpine metamorphic overprint was not strong enough to erase pre-Alpine isotopic signatures and mineral ages (Neubauer et al., 1994; Dallmeyer et al., 1998).

Although the zircon age data are decisive to resolve the tectonics of the Noric Nappe, we start with the description

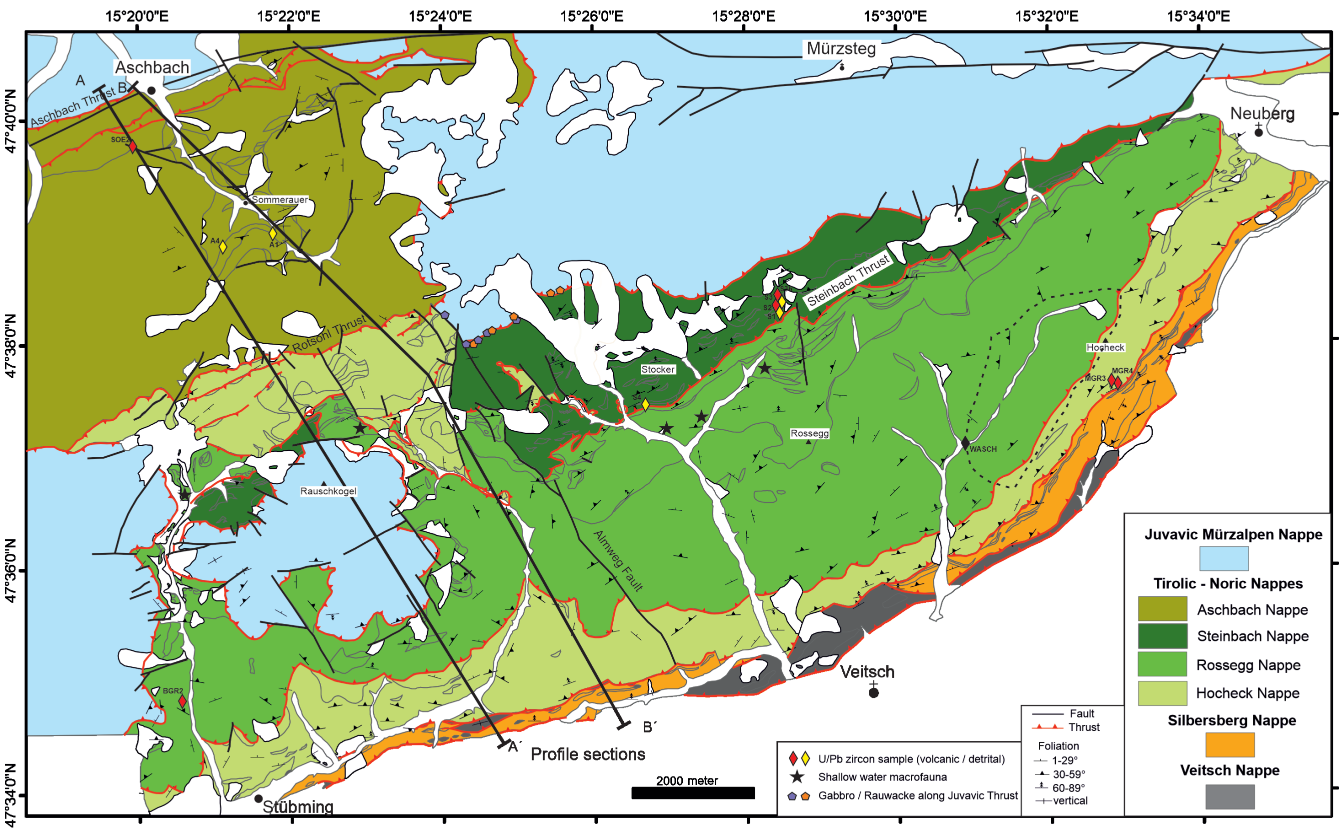

Figure 3: Structural map of the study area with name-giving locations, sampling spots and fossil findings. Locations of cross sections (Fig. 4) are indicated.

of the Noric Group (chapter 3), present the zircon age data (chapter 4), explain the tectonic structure (chapter 5) and discuss the initial arrangement of the sedimentary facies realms and its regional significance (chapter 6).

3. Lithostratigraphy and sedimentary facies of the Noric Group

3.1 Blasseneck Porphyroid (Early to Late Ordovician)

The Blasseneck Porphyroid is the result of an extended Ordovician magmatic event which is present in many units in the Eastern and Southern Alps (Heinisch; 1980, 1981); type locality is the Blaseneck mountain (Hubmann et al., 2014) ca. 60 km west of the Veitsch area. The Blasseneck Porphyroid of the Veitsch area consists mainly of crystal-rich meta-ignimbrites of dacitic composition (Heinisch, 1980). Frequent intercalations of fine-grained siliciclastic rocks as depicted by Cornelius (1936) cannot be confirmed. The two-phase low-grade metamorphism has wiped out most volcanic textures, transformed the original glassy matrix into fine-grained secondary minerals like sericite, chlorite, quartz, albite and kaolinite (Heinisch, 1980) and affected also the phenocrysts (sericitization of feldspar, plastic deformation and dynamic recrystallisation of quartz, dissociation of biotite). Deformation has induced a foliation of various intensity, from nearly absent in massive porphyroids to mylonitic textures near the Noric Thrust.

The thickness varies from ca. 300 m at Sommereck near Aschbach to > 700 m in the central part of the study area. The Blasseneck Porphyroid is covered mainly by fine-grained metasediments deposited on a flat surface without significant relief. Locally, quartz phenocrysts are concentrated by reworking of unconsolidated volcanic material (Fig. 5), sometimes alternating with phyllites of the Rad Formation (Nievoll, 1983).

3.2 Stocker Formation (Early Ordovician to Silurian)

The Stocker Formation was initially described as a subunit of the Rad Schists (Nievoll, 1987), mentioned under „Remarks“ of the Rad Schists by Hubmann et al. (2014) and described as a formation by Nievoll and Suttner (2015). The name is derived from the locality Stocker (Fig. 2: 15.445E; 47.630N; all coordinates in decimal degrees) where metavolcanics and metavolcaniclastics are abundant; the type section is located in the Steinbachgraben between 1030 and 1190 m above sea-level. Total thickness is ca. 500 m. The contact to the Kaskögerl Formation in the footwall is tectonic, the contact in the hangingwall to a second level of the Kaskögerl Formation is stratigraphic (Figs 5-6). The lowermost part of the Stocker Formation consists of phyllites with intercalated layers and lenses of sandstones and quartzites (Figs 6-7a,b). Locally, well-preserved slump structures indicate upright position (Fig. 7c). The middle part of the Stocker Formation is

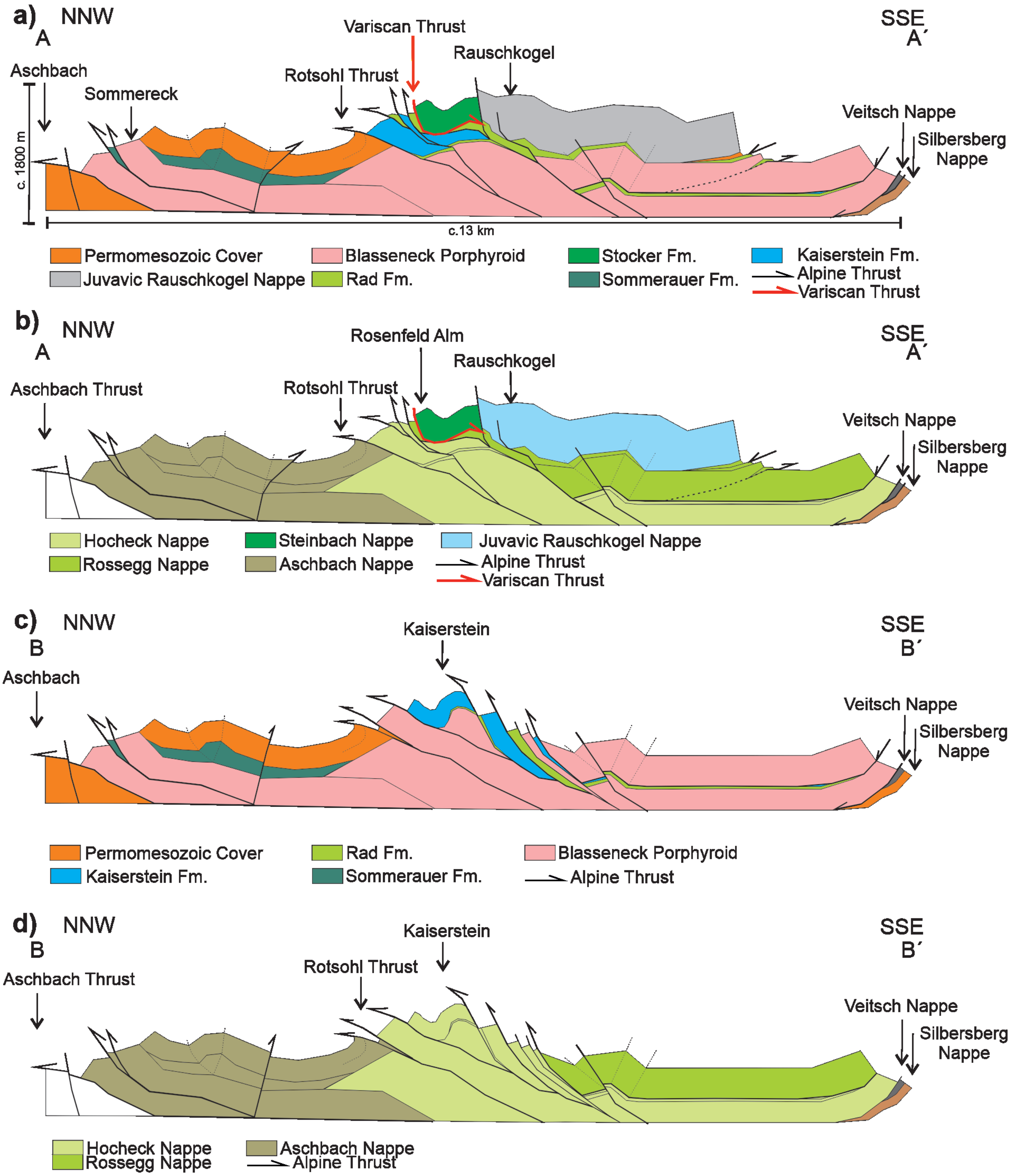

Figure 4: Cross sections across Rauschkogel Klippe **(a-b)** and Kaiserstein **(c-d)**. For location of sections see Fig. 3. Profiles (**a)** and (**c)** show formations with simplified lithologies; in (**b**) and (**d)** individual nappes are displayed. Note two-phase tectonic evolution with Variscan thrusts in red and eo-Alpine thrusts in black.

characterized by thin layers and lenses of metavolcanics and metavolcaniclastics. The metavolcanics are < 10 m thick, chemically of intermediate composition and were erupted as lava (Nievoll, 1983). Secondary minerals of the fine-grained matrix are sericite, chlorite, quartz and carbonate. Phenocrysts < 4 mm are mainly plagioclase, an unknown mafic mineral transformed into chlorite aggregates and, very rarely, also quartz. Two levels of metavolcanics are exposed in the type section and one level in the Preisenbachgraben 1 km to the southwest.

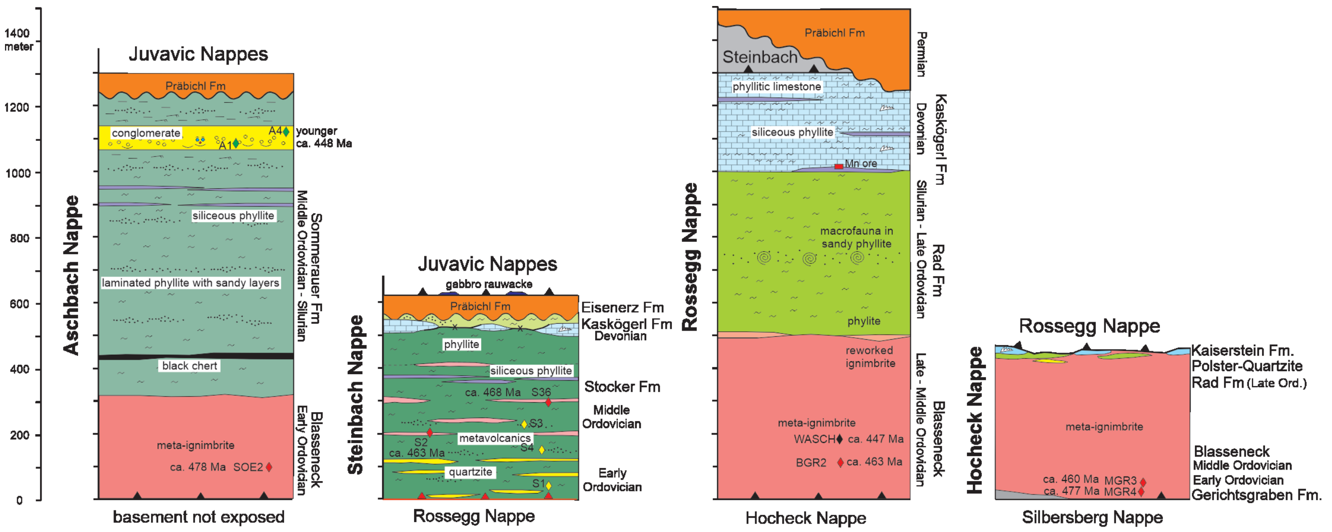

Figure 5: Schematic columns of lithologies distributed in different nappes including formation names, estimated thicknesses, supposed stratigraphic age range and distribution of U/Pb zircon age data (red for meta-volcanics, yellow for sandstones). Levels containing biostratigraphic data (macrofauna given by spirals and conodonts findings symbolized by jagged, ramiform conodont type) are indicated. Thrusts are marked with thick triangle ornamented lines. Red triangles at the base of the Steinbach Nappe denote the Variscan Steinbach Thrust (Fig. 3).

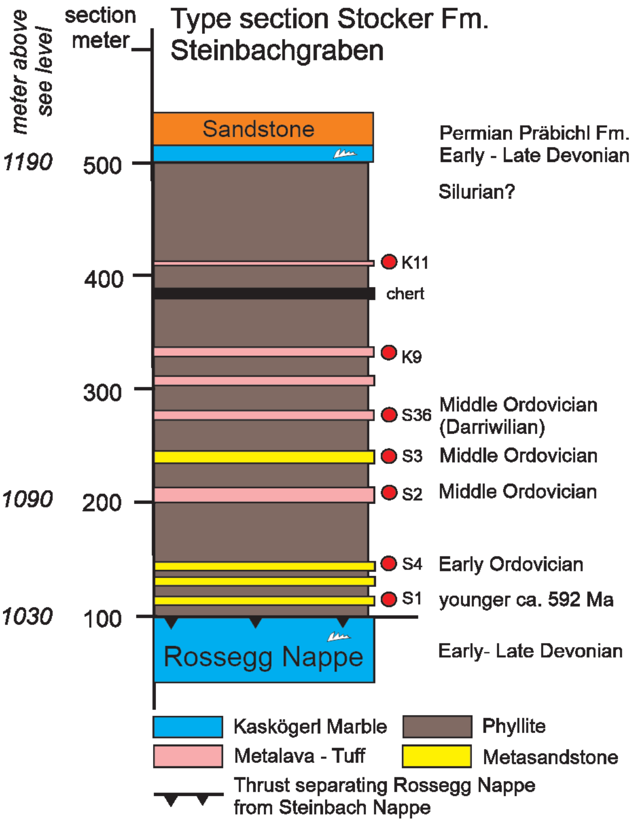

Figure 6: Type section of the Stocker Formation in the Steinbachgraben with supposed deposition ages of metasandstone, metalavas and tuffs (for location see Fig. 2). Position of dated samples (S1, S2, S4, S36) and lithologies described in the text are given. Samples K9 and K11 derived from the Kaiblinggraben, ca. 2000 meter to the west of Steinbachgraben and were projected into the profile.

The thickness of the metavolcaniclastics ranges between a few centimeters to several meters and comprises former ash tuffs, crystal-rich tuffs and lapilli tuffs of rhyolitic composition, with obvious indications of turbulent flow, incorporation of mud clasts and re-sedimentation. Lapilli are sorted or unsorted and reach < 30 mm in diameter. In the Kaiblinggraben about 2 km east of the Steinbachgraben, a breccia layer of 3 m thickness is exposed which contains ca. 30 % lithic components, both volcanics and phyllites, ca. 20 % porphyric quartz grains and ca. 50 % sericitic matrix (Figs 7e,f). In the upper 150 m of the Steinbachgraben section an input of volcaniclastics is no more evident. Here, phyllites are prevailing, intercalated with black, siliceous phyllites of < 1 m thickness. The depositional environment in the lower and middle part of the Stocker Formation has been unstable, as deduced from the heterolithic composition, the presence of slump structures and the breccia layer. The upper part was apparently deposited in quiet, offshore conditions without significant features.

3.3 Rad Formation (Late Ordovician to Silurian)

The name of this formation is derived from "Wirtshaus Rad" (Cornelius, 1936, 1952), i.e. Rudolf Lammer´s inn „zum Radwirt" (15.439E; 47.621N), demolished in the late 1930s. The position of the rebuilt, actual "Radwirt" shifted 1.25 km to the southeast into an area where Blasseneck Porphyroid is exposed and is not identical, as described by Hubmann et al. (2014), with the original location of the "Wirtshaus Rad".

The Rad Formation (Nievoll and Suttner, 2015) has a thickness of ca. 500 m and consists of uniform phyllites, with sometimes quartz- and phyllosilicate-rich layers alternating in the mm-scale. A sedimentary contact exists with the underlying Blasseneck Porphyroid as well as with the overlying Kaskögerl Formation. Typical for the Rad Formation in the Veitsch area is a layer of phyllites and metasiltstones ca. 250 m above the Blasseneck Porphyroid which contains a fauna dominated by bryozoans and accompanied by brachiopods and

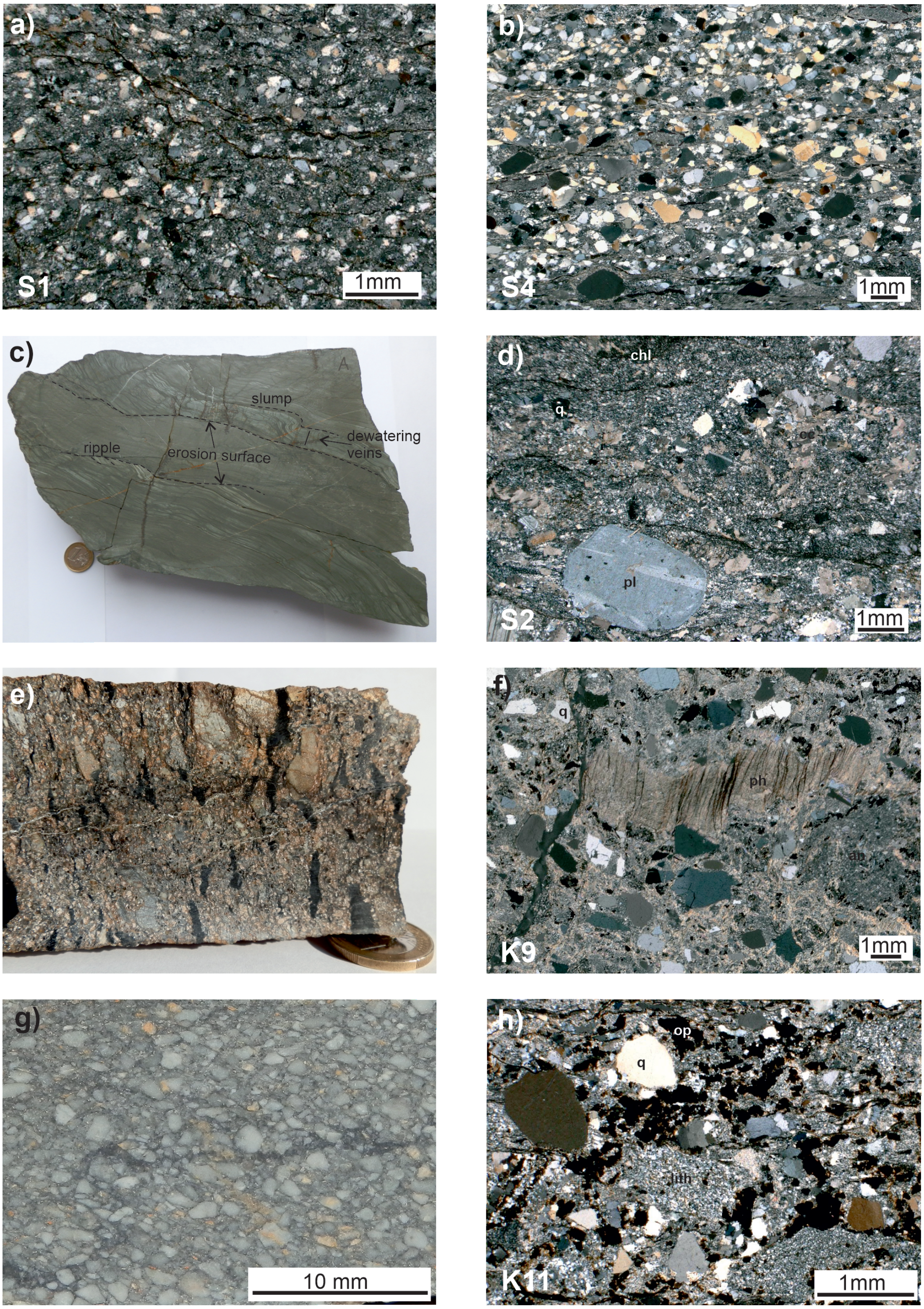

Figure 7: Thin sections and polished hand specimen of typical lithologies from the Stocker Formation (for relative stratigraphic position of samples see Fig. 6, for U/Pb age data see Figs 9-10). **(a)** Massive sandstone S1 containing monocrystalline and few polycrystalline quartz grains floating in quartz dominated matrix; feldspar is extremely rare and lithic components are absent. **(b)** Thin section of sandstone sample S4 showing mild grading. Conspicuous is first appearance of porphyric quartz and up to mm-sized lithic andesite components (some are marked by stippled lines) concentrated in distinct layers. **(c)** Example of mud- siltstone from lower / middle segments of the Stocker Formation. Dynamic conditions of deposition is suggested from slump structures, ripples and erosional surfaces. **(d)** Thin section of andesite S2 with porphyric plagioclase (pl) and quartz phenocrysts (q) floating in fine grained matrix. Secondary modification is evident from chlorite flakes (chl) after hornblende(?) and precipitation of secondary calcite (cc). Hand specimen **(e)** and thin section **(f)** from the breccia horizon (sample K9) with lithic andesite (an) and phyllite components (ph) and angular quartz grains (q). Secondary sericite has grown on expense of feldspar. **(g)** Lapilli tuff from middle section of the Stocker Formation. **(h)** Sample K11, from top part of the sequence is extremely rich in lithic components (lith), both andesite and more acidic quartz-rich clasts (dacite) and porphyric quartz (q). The matrix is rich in quartz, secondary carbonate, opaque components (op) and some mica grown along foliation planes.

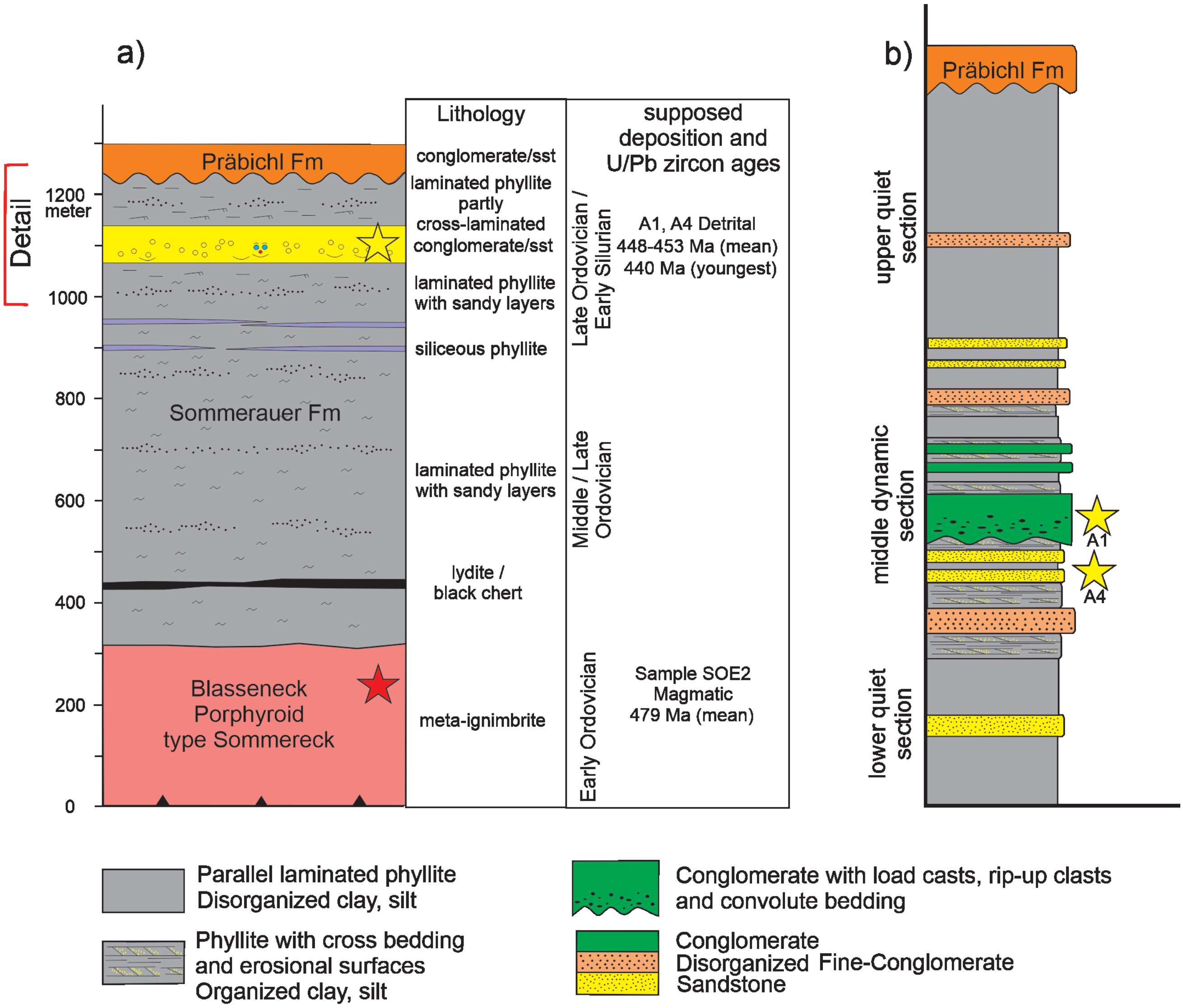

Figure 8: Schematic section of the Sommerauer Formation **(a)** with detail of the turbiditic sequence **(b)**. The terms organized and disorganized clay, silt and conglomerate refer to the classification of deep-water facies rock suites by Pickering et al. (1986). For location of the detail section and dated samples see Figure 2. Stars indicate position of dated samples.

cystoids (Figs. 2-5). This fauna, not yet described in detail, resembles at first sight Late Ordovician macrofossils from the Carnic Alps (Schönlaub and Flajs, 1993; Schönlaub, 2000). Above the fossil-bearing layer another 250 m of phyllites, again sometimes with a diffuse layering, are following. Approaching the Kaskögerl Formation in the hangingwall, dark-coloured siliceous phyllites are occurring and the phyllites are grading into phyllitic limestones.

3.4 Sommerauer Formation (Middle Ordovician to Devonian?)

The metaclastics on top of the Blasseneck Porphyroid exposed in the Rotsohl valley south of Aschbach are, due to their special sedimentary features, described as a new lithostratigraphic formation, the Sommerauer Formation. It is named after the Sommerauer farm located 2.3 km south of Aschbach (15.355E; 47.654N; Fig. 2), its footwall is the Blasseneck Porphyroid (type Sommereck) and its hangingwall the Präbichl Formation (Figs 4-8). It comprises phyllites, siliceous phyllites, lydites (black cherts), quartzites, metasandstones and fine-grained metaconglomerates. Characteristic are the following features:

– Phyllites frequently contain thin quartz-rich layers of 1 to 40 mm thickness. Quartz-rich layers < 2 mm thickness are parallel-laminated. Layers > 2 mm vary laterally in thickness, show low-angle cross lamination and soft-sediment deformation (Figs 9a,b).
– Quartzites are bedded from several cm to several dm thickness; in some outcrops dish structures and convolute bedding (Fig. 9c) indicating upright position can be observed. Some beds contain phyllite clasts (rip-up clasts) up to 10 cm in size (Fig. 9d) and bedding planes with load casts and flute marks (Fig. 9e).
– Metasandstones and fine-grained metaconglomerates form lenticular bodies of < 60 cm thickness, sometimes graded (Fig. 9f), and contain quartz grains

and lithoclasts < 6 mm and phyllite clasts < 10 cm in size. Quartz grains are predominantly monocrystalline and have partly preserved the shape and embayments typical for those formed in silicic volcanics; polycrystalline quartz grains with mylonitic texture are rare. The lithoclasts consist of metasandstone, lydite (angular grains of black chert, > 98 % SiO_2 in scanning electron microsope (SEM) analysis), and metavolcanics (> 71 % SiO_2 in SEM analysis) (Fig. 9g). When intercalated in phyllites, coarse sandstones and fine-grained metaconglomerates are weathering out as tongue-shaped bodies; in one outcrop convolute bedding is preserved. Such rocks are not quartz-cemented and contain < 10 % carbonate disseminated in the matrix.

– Siliceous phyllites occur together with phyllites in the vicinity of Sommerauer farm, lydites occur near Sommerhaus 0.5 km south of Aschbach and in the Dürrwald valley (2.5 km east of Aschbach, Fig. 2). Bed thickness in the siliceous phyllites is 1-5 cm, in lydites 10-50 cm. In thin section of lydites, circular structures of < 0.15 mm diameter have been interpreted as relics of radiolarians (Cornelius, 1952). Such structures are also present in angular lydite grains of metaconglomerates (Fig. 9h).

The total thickness of the Sommerauer Formation is estimated as 700-1000 m, with laminated phyllites forming the major part. The quartzites with intercalated coarse metasandstones and fine-grained metaconglomerates are about 100 m thick. The siliceous phyllites and lydites are < 10 m thick.

Sedimentary structures like dish structures and convolute bedding (e.g., Tinterri et al., 2016) in metasandstones and quartzites, bedding planes with load casts and flute marks (e.g., Peakall et al., 2020), tongue-shaped bodies of sandstones and fine-grained metaconglomerates intercalated in phyllites which are interpreted as flame structures (e.g., Butler et al., 2016), point to deposits of turbidites. Preservation of monocrystalline quartz grains typical for those in silicic volcanics and angular lydite grains indicate rapid transport across the shoreface. Phyllites containing thin quartz-rich layers with parallel lamination and low-angle cross-stratification represent former mixed sand-mud bedforms (Baker and Baas, 2020). This facies is attributed to outer, distal parts of a submarine fan (e.g., Spychala et al.; 2017, 2020), while the coarse-grained facies is attributed to the proximal lobe (e.g., Brooks et al., 2018).

3.5 Kaskögerl Formation (Early to Late Devonian)

For the Veitsch area, the term Metalliferous Limestones (Hubmann et al., 2014) was replaced by the Kaskögerl and Kaiserstein Formations, respectively (Nievoll and Suttner, 2015). The Kaskögerl Formation, named after the Kaskögerl (15.481E; 47.636N) (Fig. 2), consists of banded limestones to calcitic marbles and phyllitic limestones of < 300 m thickness; siliceous to cherty layers are frequent at but not restricted to the contact with the underlying Rad Formation. The Kaskögerl Formation occurs in two levels. The lower level is overlain tectonically by the Stocker Formation while the higher level is transgressively overlain by the Präbichl Formation. The stratigraphic range as proved by conodonts is Lochkovian to Famennian (Ebner, 1974; Nievoll, 1987; Nievoll and Suttner, 2015) with the fauna best preserved in Middle and Late Devonian limestones rich in organic substance. The Kaskögerl Formation is interpreted to have been deposited in a pelagic basinal environment.

3.6 Kaiserstein Formation (Early Devonian)

The Kaiserstein Formation, named after the Kaiserstein mountain (1322 m; 15.381E; 47.622N) (Figs 2-4) represents predominantly light-colored, massive to thick-bedded calcitic marbles of < 140 m thickness. In the western part of the study area also marbles of light red to violet color containing crinoidal detritus occur. Conodonts are very rare and have been determined up to now as Lochkovian only (Ebner, 1974; Nievoll, 1987). The footwall of the Kaiserstein Formation consists of Blasseneck Porphyriod, Rad Formation, but also Präbichl Formation; in all cases a tectonic contact is evident. The original hangingwall is made up of the Präbichl Formation as indicated by breccias rich in marble components, now overthrusted. Based on the aspect of the marbles the sedimentary facies is assumed to be shallow water, near-reef.

4. Geochronological, geochemical and petrographic investigations

4.1 Sampling

U-Pb zircon age data targeted five Blasseneck Porphyroid localities to get a more comprehensive picture of its stratigraphic position and age range. Five metavolcanic and metaclastic samples of the Stocker Formation were processed to establish its time relationship with the Blasseneck Porphyroid volcanism and/or define maximum depositional ages. Two samples were taken from metaclastics of the Sommerauer Formation, to identify its source and maximum depositional ages. Coordinates and analytical data of the 12 zircon samples are shown in the Appendix (Tab. A1) and the supplementary material (Tab. S1). A selection of Blasseneck Porphyroids (8 samples, 4 of them dated by U/Pb zircon chronology) and Stocker metavolcanics (3 samples, one of them dated) was analyzed geochemically. Sample locations and analytical data are given in the Appendix (Tables A1, A2). The petrography of samples selected for zircon age dating and of ca. 100 metaclastics and metavolcaniclastics was investigated in thin sections.

4.2 Geochemistry

4.2.1. Analytical procedure

Powdered samples were dried at 105°C at least for two hours before loss on ignition (LOI) was obtained at

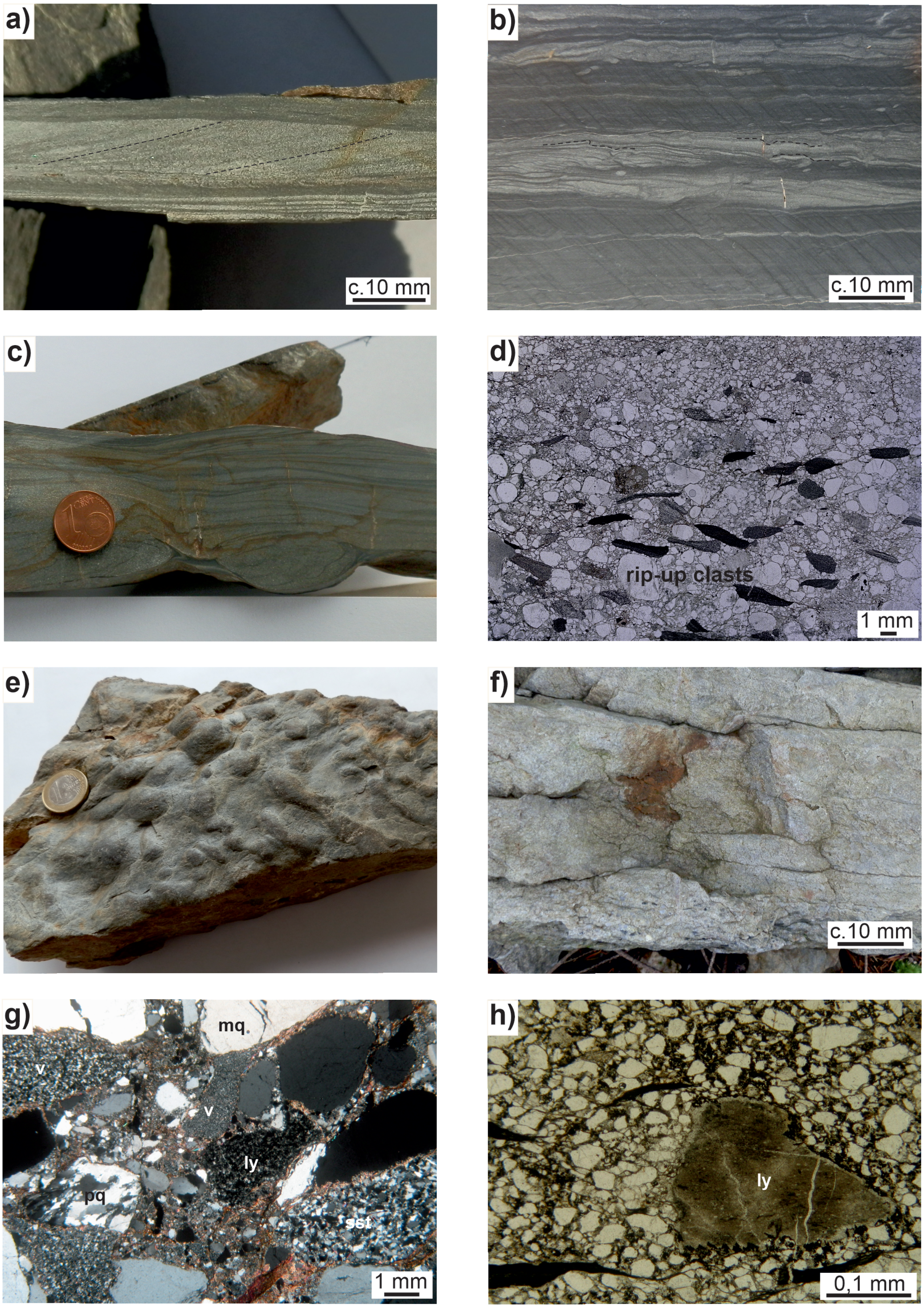

Figure 9: Lithologies and sedimentary structures of the turbiditic part of the Sommerauer Formation; see also Figure 8b. **(a)** Parallel-laminated phyllite with low-angle cross-laminated siltstone. **(b)** Soft sediment deformation (stippled) and cross-lamination in siltstone. **(c)** Hand specimen with flute marks. **(d)** Basal part of a turbiditic fine-conglomerate with grading and rip-up clasts (predominately phyllite lithologies). **(e)** Load casts and flute marks in loose blocks of the Sommerauer Formation. **(f)** Fine-conglomerate / sandstone beds with grading and rip-up clasts in basal portions (black elongated clasts). **(g)** Lithoclasts in coarse sandstone with monocrystalline (mq) and polycrystalline, mylonitic quartz (pq), various meta-volcanics (v), metasandstone (sst) and lydite (ly). **(h)** Clast of lydites (ly) with circular structures (white spots) probably representing radiolarians.

1030°C and preparation of fused glass discs. A lithium tetraborate/metaborate mixture was used (7 gram) together with 1 gram of sample to produce the glass beads which were measured for major, minor, and selected trace elements with a Bruker Tiger S8II at the Institute of Earth Sciences - NAWI Graz Geocenter, University of Graz. Calibration curves for the analyzed elements were obtained by measuring approximately 100 international reference materials (United States Geological Survey, SGS Reference material services, Geological Survey of Japan, Centre de Recherches Petrographiques et Geochimiques, International Association of Geoanalysts). Counting times on peak and each background were max. 100 seconds per element, a variable alpha correction was applied to correct for matrix effects. The lower limit of detection (LLD) for most elements is in the range of 10 to 30 mg/kg, uncertainties for elements with a concentration >10 wt % is <1 %, for elements between 10 to 0.1 wt % ca. 1-3 % and for elements <0.1 % approximately 5 %. Sample coordinates and analytical data are provided in the Appendix, Tables A1 and A2.

4.2.3. Results

To our 11 new samples we add 17 published analyses of the Blasseneck Porphyroid from the study area (Heinisch, 1980) and 8 unpublished analyses of metavolcanics of the Stocker Formation carried out at the Quality Management Department of RHI Magnesita´s Veitsch plant (no trace element data are available from that data set). The purpose of our chemical analyses was mainly to classify the metavolcanic rocks correctly, not a detailed geochemical study. The alteration of mineral phases of the Blasseneck Porphyroids is very variable. Those rocks exposed close to eo-Alpine thrusts experienced mylonitization and fluid infiltration, frequently associated with transformation of feldspar to white mica (e.g., samples MGR4 and BGR2). Other samples, such as SOE2 preserved magmatic textures, although even here sericitisation is common. Despite of this, loss on ignition (LOI) is small in the Blasseneck Porphyroids (1.3-2 % with one outlier of 4 %). The Stocker metavolcanics represent, by contrast to the Blasseneck Porphyroids, thin layers embedded within the sedimentary sequence. A possible interaction with the host rock is high and indeed, some samples exhibit high percentage of LOI. The comparatively high LOI of the two samples S2 and S33 with 6.61 and 6.98 % LOI is explained by the content of secondary carbonate in these samples. In summary, element mobility cannot be excluded, especially for the major elements.

In the Total Alkali against Silica (TAS) classification diagram of Le Bas et al. (1986) the majority of the Blasseneck Porphyroid samples plot in the dacite field and two samples (MGR4, SOE2) in the rhyolite field (Fig. 10a). The metavolcaniclastics of the Stocker Formation have rhyolitic composition whereas the two metavolcanics (S2 and S33) plot in the andesite field. In the SiO_2 - K_2O plot of Peccerillo and Taylor (1976) the Blasseneck Porphyroid samples fall into the calc-alkaline and high-K calc-alkaline series, while the Stocker metavolcanics follow the calc-alkaline series with the exception of the two andesitic samples, which lie in the tholeiite series field (Fig. 10b). However, these two samples have unusual low K_2O and high Na_2O values and fall in the FeOt/MgO vs. SiO_2 diagram (Miyashiro, 1974) into the calc-alkaline group (Fig. 10c). With the exception of one sample, all igneous rocks are peraluminous; most samples have A/CNK values larger than 1.1 (Fig. 10d), which is typical for magmatics with S-type affinity (Chappell and White, 2001). In Figure 11 the selected major and trace elements of the investigated samples are plotted against SiO_2. TiO_2 and FeOt decrease with increasing SiO_2 content, typical for calc-alkaline rocks (Maaløe and Petersen, 1981). Al_2O_3, K_2O, and Na_2O also show decreasing trends with increasing SiO_2 indicating fractionation of feldspars. The decrease in P_2O_5 and Zr can be explained by crystallization of apatite and zircon. A number of samples have unusual high concentrations of Zr (>250 mg/kg) which is significantly higher than calculated zircon saturation contents after Watson and Harrison (1983) indicating incorporation of xenocrystic zircons in the parental magma. Rb and Sr do not display well developed trends; however, a few samples have elevated contents with values >300 mg/kg.

4.3 Geochronology

4.3.1. Analytical procedure

Zircons were separated by crushing 2.5-3 kg of each sample and concentrating the heavy mineral fraction in a Conrad gold pan. The heavy mineral fraction was then separated using a Frantz magnetic barrier separator and zircon grains were handpicked randomly, mounted in epoxy resin and polished to expose the grain interiors. Cathodoluminescence (CL) images of zircons were obtained by a JEOL JXA-8530F Plus EPMA to identify internal growth patterns, homogenous areas for dating and possible inclusions. Zircon dating was performed with an ESI NWR 193 nm laser ablation system coupled to a Nu Plasma II multi-collector inductively-coupled plasma mass spectrometer (MC-ICP-MS) at the NAWI Graz Central Lab Water, Minerals and Rocks (Graz University of Technology and University of Graz). Line scans were used for dating samples A1, A4 and WASCH, while spot ablation was carried out for all other samples. The measurement conditions for both methods, analytical data and selected CL images are shown in the Appendix and the supplementary material (Fig. S2 and Table S1). Analytical procedures for the line scans are described in more detail in Mandl et al. (2018) and Haas et al. (2020). For the line scan, the Plesovice zircon (Sláma et al., 2008) and for spot measurements, the GJ1 zircon (Jackson et al., 2004) was used as the primary reference material and/or the 91500 (Wiedenbeck et al., 1995), M257 (Nasdala et al., 2008), Plešovice (Sláma et al., 2008) and Mud Tank (Black and Gulson, 1978; Gain et al., 2019) zircons were used as secondary reference materials to monitor the reproducibility and accuracy of the analyses. Spot ablation was performed with 35 or 15 µm spot diameter, 5 Hz repetition rate, and 20% of 5 mJ

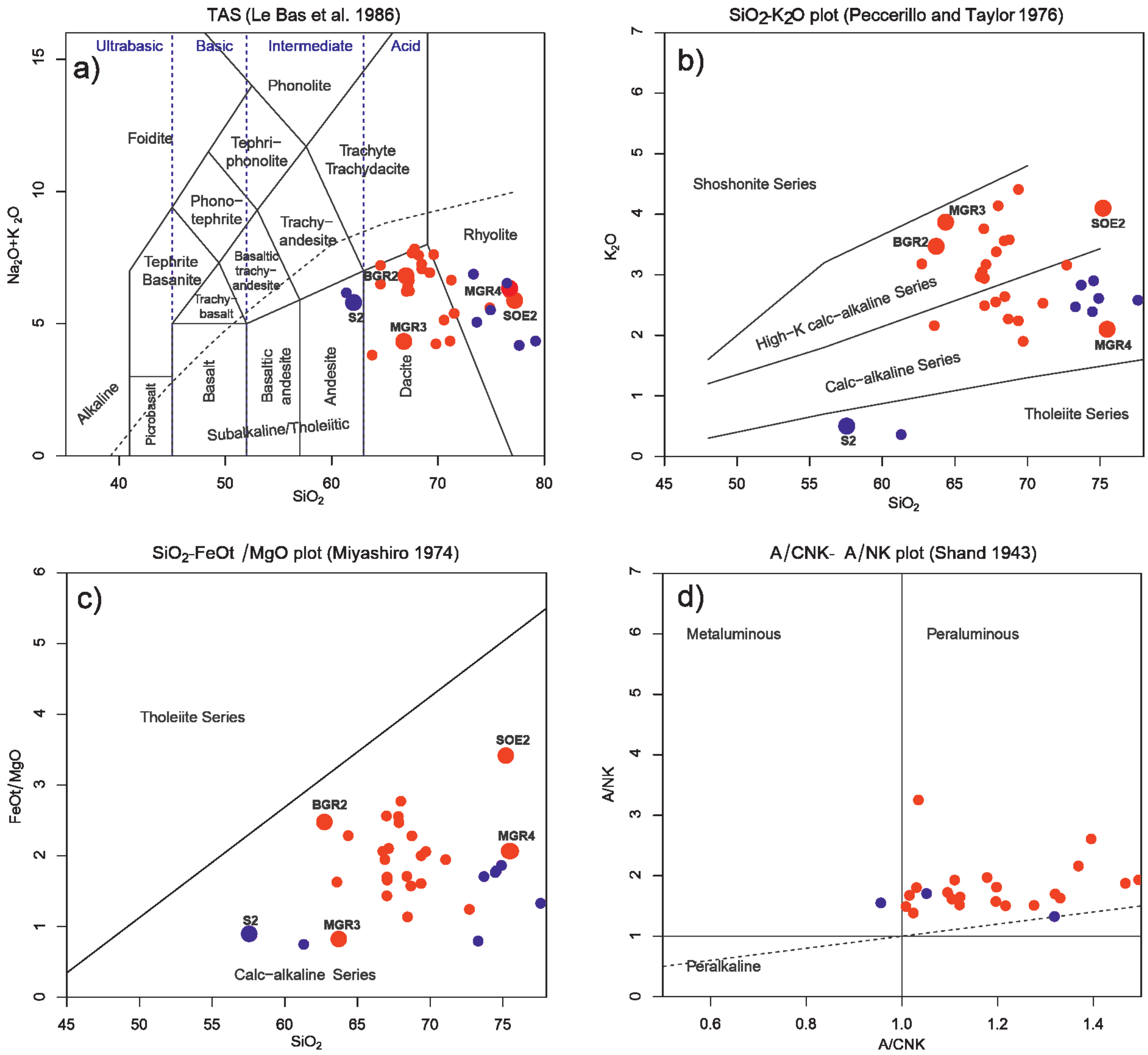

Figure 10: Classification diagrams of Blasseneck Porphyroids (red symbols) and Stocker metavolcanics (blue symbols). Labelled large symbols represent samples dated by U/Pb zircon chronology. **(a)** TAS classification diagram after Le Bas et al. (1986); **(b)** SiO_2 / K_20 plot after Peccerillo and Taylor (1976); **(c)** FeOt/MgO vs. SiO_2 diagram (Miyashiro, 1974); **(d)** A/CNK after Shand (1943). For explanation see text.

energy output resulting in a sample fluence of 2.5-2.7 J/cm^2. The length of the scan line varied between 50 and 150 µm with a spot diameter of 10–15 µm, 7–10 Hz, a scan speed of 10 µm s^{-1} and a maximum laser energy of 5.0 to 5.5 J cm^{-2}. Gas blanks were acquired for 25s during laser warm-up, which was followed by 15s of sample ablation for spot analyses. The accuracy of the secondary standards Plesovice, 91500, M257 and Mud Tank was better than 1.2 %. The long-term variance of validation material is about 1.3 %. A common lead correction was not applied to the results. Data were reduced with the IOLITE v. 3.71 software package using the U_Pb_Geochron4 data reduction scheme (Paton et al., 2010; 2011) and, for line scans, using the MS Excel spreadsheet LamTool U-Th-Pb version VI (Košler, 2008). Concordia diagrams and ^{206}Pb/^{238}U weighted mean calculations were prepared with IsoplotR (Vermeesch, 2018). ^{206}Pb/^{238}U weighted mean ages of the samples were calculated from single zircon dates showing less than 2 % discordance. External uncertainties were propagated to the internal 2σ error of the weighted mean ages by quadratic addition (external error propagation, EEP) (Horstwood et al., 2016). Since the minority of our single crystal ages (ca. 11 %) is older than 1100 Ma and the cut-off in our Kernel density estimation (KDE) plots is 1200 Ma, we refrain from using ^{207}Pb/^{206}Pb ages for those older grains. However, these data together with single grain ^{207}Pb/^{235}U, ^{206}Pb/^{238}U and single grain Concordia ages are given in the supplementary material (Tab. S1). Single grain ages mentioned in the text below are single grain Concordia ages.

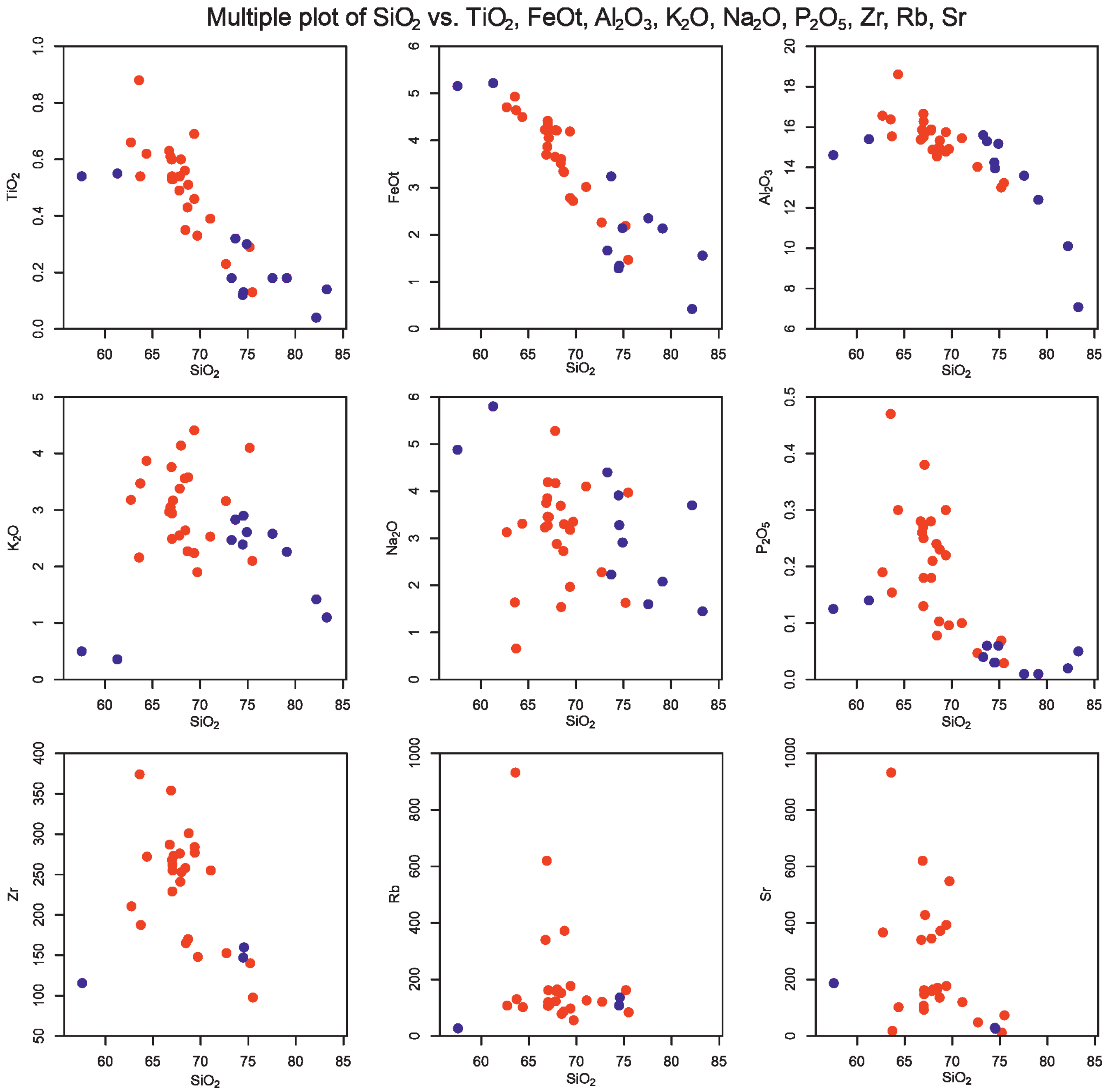

Figure 11: Selected major and trace elements plotted against SiO_2. Blasseneck Porphyroids in red and Stocker metavolcanics in blue symbols. For explanation see text.

4.3.2. Results

4.3.2.1. Blasseneck Porphyroid

Sample "***WASCH***" from Taurisgraben (15.513E; 47.618N) was the starting point of our geochronological study. The intention was to confirm published Blasseneck Porphyroid ages from the Kitzbühel (Söllner et al., 1991; 1997; Blatt, 2013) and Eisenerz areas (Söllner et al., 1997). The catchment area of Taurisgraben is about 4 km^2 and built exclusively of Blasseneck Porphyroid draining about 500 m in thickness (Figs 2-3). Given the abundance of zircon grains in Taurisgraben river sand we used a Conrad gold pan for zircon enrichment. A total of 29 zircons with a grain size between 200-600 µm were analyzed. One zircon grain (grain 29, see supplementary material) with an age of ca. 1873 Ma (single grain Concordia age) is slightly discordant and another 4 grains between ca. 686 Ma and 530 Ma are considered as xenocrysts (grains 25-28). The remaining 24 grains give a Concordia age of ca. 447 Ma (Fig. 12a). For weighted mean age calculation, we omitted the 5 xenocrysts, one outlier (grain 22) and the youngest two zircons (grains 1, 2) for possible lead loss. The remaining 21 zircons give an $^{206}Pb/^{238}U$ weighted mean age of 444 ± 1.2 Ma. Applying external error propagation (EEP) gives an age of 444 ± 5.9 Ma (Fig. 12b). Long- to short-prismatic zircons have oscillatory zoning. This surprisingly young age raised doubts of a coeval

Blasseneck Porphyroid "event" along the entire (Eastern) Greywacke Zone and led us to sample more localities of the Blasseneck Porphyroid across the study area.

Sample ***BGR2*** (15.343E; 47.581N) at the western end of the study area is a strongly deformed metadacite with a high content of fine-grained, sericitic matrix, monocrystalline quartz phenocrysts and relics of feldspar, hornblende and biotite phenocrysts (Fig. 13a). A total of 29 zircons were analyzed, one of them with more than 2 % discordance (grain 12) was dismissed. The remaining 28 zircons give single zircon ages between 455 Ma and 475 Ma, quite evenly distributed along the Concordia with a Concordia age of ca. 463 Ma (Fig. 12c). The main group of zircons overlapping in errors (grains 8-23) give a $^{206}Pb/^{238}U$ weighted mean age of 464 ± 0.6 Ma (464 ± 6 Ma with EEP) (Fig. 12d). The youngest 6 zircons give a $^{206}Pb/^{238}U$ weighted mean age of 456 ± 1.1 Ma (± 6 Ma with EEP) interpreted to date closely the age of volcanic eruption. The size of short-prismatic, pink zircons is 150 to 200 µm; the aspect ratio is 2:1 to 3:1. All zircons show oscillatory zoning patterns; the Th/U ratios range from 0.21 to 0.57 (mean 0.35) as characteristic for a magmatic origin (Rubatto, 2002).

Sample ***MGR3*** (15.547E; 47.627N) is a strongly deformed metadacite south of Hocheck with partly recrystallized quartz phenocrysts up to 1 mm in size. The few quartz phenocrysts which escaped recrystallization exhibit resorbed embayment typical for solution processes within the magma chamber. Feldspar phenocrysts are, like in sample BGR2, mostly transformed to sericitic mica (Fig. 13b). A total of 30 zircons were analyzed, all of them have less than 2 % discordance. The size of long- to short-prismatic zircons with aspect ratio from 1.6:1 to 3.5:1 is between 100 and 200 µm. Pink zircons with oscillatory zoning and Th/U ratios > 0.1 (mean 0.35) are characteristic for a magmatic origin (Rubatto, 2002).

Two zircons (grains 29, 30) with Concordia ages of 488 and 490 Ma are interpreted as xenocrysts. The youngest zircon (grain 1) with ca. 446 Ma has been omitted because of possible Pb loss. The remaining 27 zircons are distributed along the Concordia and give a Concordia age of ca. 460 Ma (Fig. 12e). Weighted mean age plots display apparently two age groups (Fig. 12f), the younger of which defined by zircon grains 2-11 give a $^{206}Pb/^{238}U$ weighted mean age of ca. 453 Ma ± 0.7 Ma (± 6 Ma with EEP). The older group of zircons (grains 12-28) give a $^{206}Pb/^{238}U$ weighted mean age of 466 ± 0.6 Ma (± 6.1 Ma with EEP). Data of both groups hardly overlap even when external error propagation is applied, hence, existence of two age groups should be considered possible in that sample (see also Kernel density estimation (KDE) plots in Figure 15). The youngest reliable zircon group of ca. 453 Ma may date closely the time of volcanic eruption.

Sample ***MGR4*** (15.548E; 47.627N) was taken from the very base of the Blasseneck Porphyroid only few meters above the Noric Thrust and 100 meters below sample MGR3. It represents a local, unusual type of crystal-poor ignimbrite of white color and rhyolitic composition (Fig. 13c). A few meters of strongly deformed phyllites separates this level from the main body of the dacitic Blasseneck Porphyroid in the hangingwall. This sample is extremely poor in zircon and has the lowest zirconium concentration (98 ppm) of all studied samples. With the standard procedure only 9 zircon crystals were extracted, three of them have 9-12 % discordance (grains 1, 8, 9). The remaining 6 zircons give a poorly defined Concordia age of ca. 477 Ma and a $^{206}Pb/^{238}U$ weighted mean age of ca. 476 Ma (Figs 12g,h). The obtained ages cannot be taken seriously but provide a hint that "older" magmatic pulses may be present within the Blasseneck Porphyroid body (see sample below). The 100 to 200 µm large pink zircons with aspect ratio between 1.5 and 2 show oscillatory zoning. Th/U ratios are between 0.3 and 0.7 (mean 0.43).

Sample ***SOE2*** (15.332E; 47.663N) from Sommereck near Aschbach is a metarhyolite with monocrystalline quartz phenocrysts, feldspar phenocrysts largely transformed into sericite and relics of pyroxene (?) (Fig. 13d). A total of 36 zircons were analyzed, all of them have less than 2 % discordance. Three zircons are considered xenocrysts that give ages of ca. 530 Ma, 520 Ma and 494 Ma (grains 34-36). One zircon with a large analytical error (grain 27) was dismissed. The remaining 32 zircons give ages between ca. 464 Ma and 486 Ma, evenly distributed along the Concordia with a mean Concordia age of ca. 478 Ma (Fig. 12i). 19 grains overlapping in error were selected for a $^{206}Pb/^{238}U$ weighted mean age calculation and give 479 ± 0.6 Ma (± 6.3 Ma with EEP) (Fig. 12j). When the youngest grain (grain 1) is dismissed for possible lead loss, the six next-younger zircons (grains 2-7) give a $^{206}Pb/^{238}U$ weighted mean age of 470 ± 0.9 Ma (± 6.3 Ma with EEP) which closely dates time of volcanic eruption. No zircons younger 464 Ma exist in that sample. Long- to short-prismatic pink zircons with oscillatory zoning have Th/U ratios from 0.17 to 0.58 with a mean of 0.33; all features point to magmatic origin.

4.3.2.2. Metavolcanics and metasandstones of the Stocker Formation

Here we sampled from the stratigraphic base to the top the type profile of the Stocker Formation in the Steinbachgraben (Nievoll and Suttner, 2015) and one sample from outside the type profile (S4). Samples S2 and S36 are metaandesites, samples S1, S3 and S4 are metasandstones.

Sample **S2** (15.474E; 47.639N) is from the lower, 8-10 meters thick andesitic layer in the Steinbachgraben section (Fig. 6). A total of 75 zircons were analyzed, two of them with more than 2 % discordance (grains 48, 74) and two outliers (grains 1, 3) have been dismissed. The remaining zircon scatter along the Concordia with a cluster of 37 grains (grains 6-42) at ca. 463 Ma ($^{206}Pb/^{238}U$ age) (Figs 14a,b). The youngest 6 zircons (outlier grains 1, 2, 3 erased) give a $^{206}Pb/^{238}U$ age of ca. 455 Ma (± 6 Ma with EEP) (see also KDE plots in Fig. 15). Long- to short-prismatic pink zircons show oscillatory zoning, few of them are rounded and have Th/U ratios from 0.6 to 2.8 with a mean of 1.2.

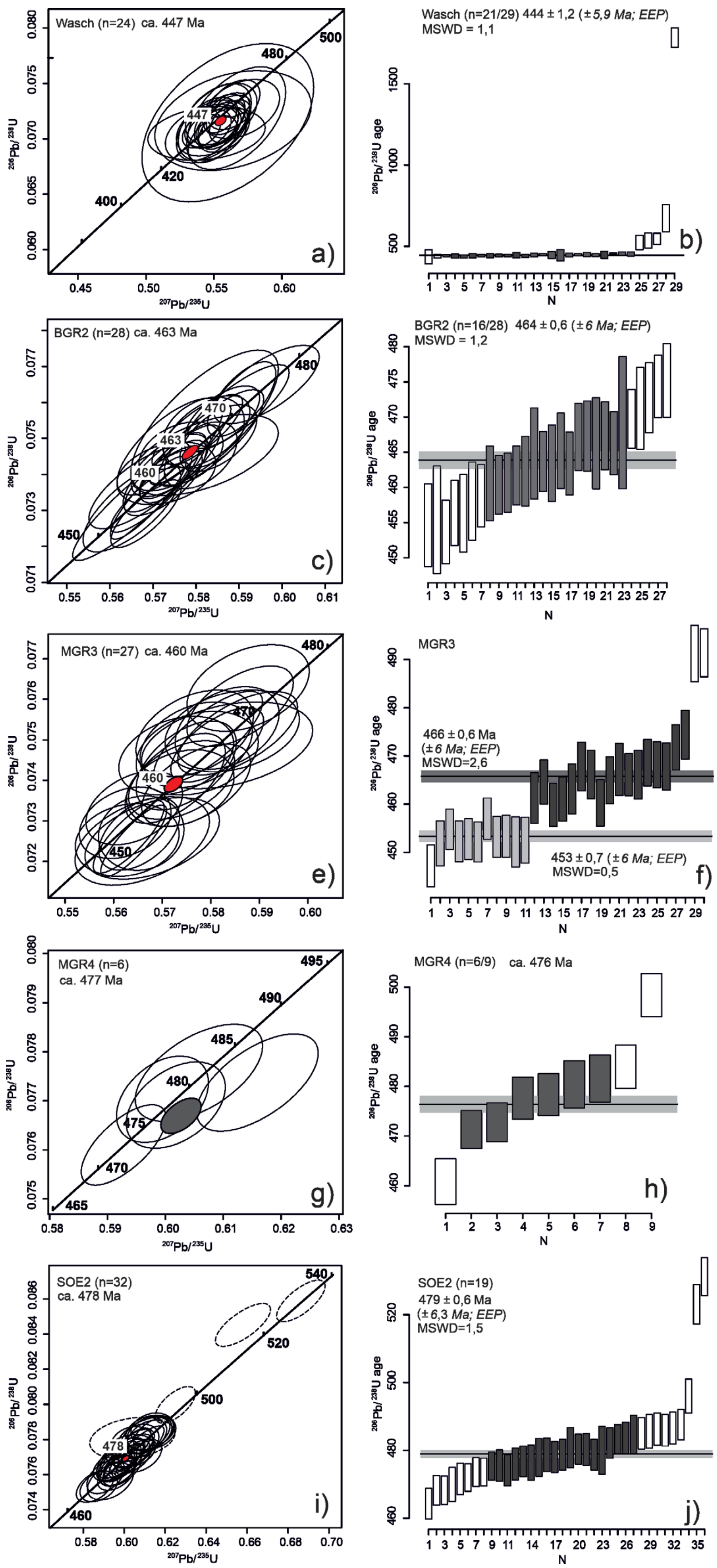

Figure 12: U-Pb Concordia ages (left row) and $^{206}Pb/^{238}U$ weighted mean ages (right row) of Blasseneck Porphyroid types. Grey shaded grains in weighted mean plots were used for $^{206}Pb/^{238}U$ age calculations. Grains given as stippled ellipses in sample SOE2 (i) are not included for calculation. Uncertainties are 2σ, errors given in Italic characters were calculated by implementing the long-term variance of validation material (1.3 %) through External Error Propagation (EEP); MSWD is Mean Standard Weighted Deviation.

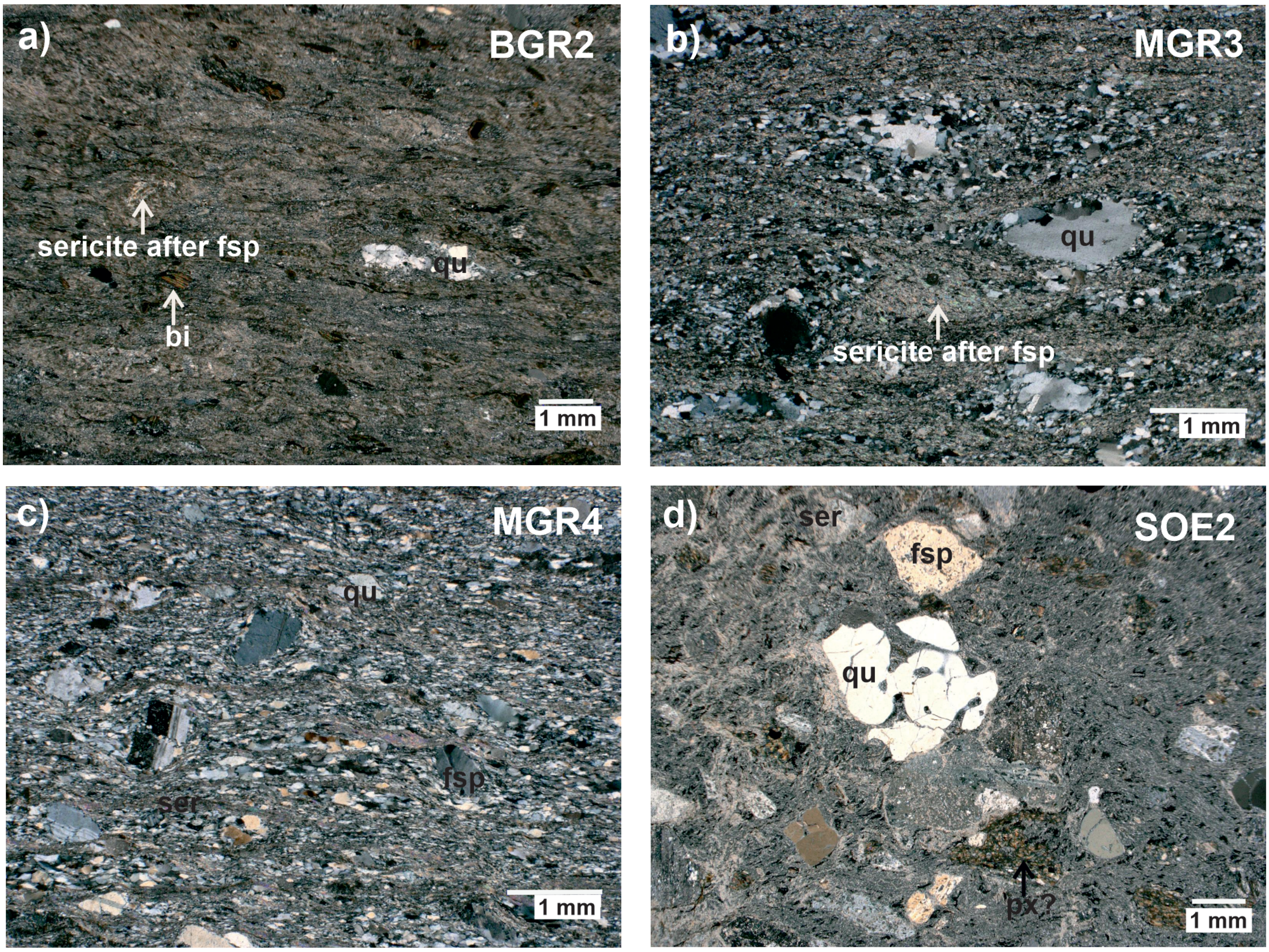

Figure 13: Thin section from dated varieties of Blasseneck Porphyroids, for sample sites see Figure 2. Abbreviations are fsp – feldspar, qu – quartz, bi – biotite, sericite – ser, px – pyroxene. **(a)** Dacite sample BGR2 with sericitic matrix, some feldspar that escaped sericitisation, monocrystalline quartz phenocrysts, and remnants of biotite flakes. **(b)** Strongly deformed dacite MGR3 with recrystallized quartz phenocrysts embedded in sericitic matric. **(c)** Rhyolite sample MGR4 taken few meters above the Noric Thrust with mylonitic fabric. Quartz is dynamically recrystallized whereas feldspar exhibits brittle deformation. Foliation planes are coated by sericite. **(d)** Rhyolite sample SOE2 with resorption embayment in quartz, feldspar partly transformed into sericite and remnants of pyroxene (?).

S36 (15.474E; 47.640N) is from the upper, 2 m thick andesitic layer in the Steinbachgraben section, about 80 m above sample S2 (Fig. 6). A total of 36 zircons were analyzed; 5 of them have more than 2 % discordance (grains 1, 33, 34, 35, 36) and were dismissed. Out of the remaining 31 grains 5 xenocrysts scatter between ca. 1070 Ma and 570 Ma and 26 zircons form an age cluster with a Concordia age of ca. 468 Ma (Fig. 14c). 24 zircons (grains 2-25) define a plateau with an $^{206}Pb/^{238}U$ weighted mean age of 468 ± 1.1 Ma (± 6.1 Ma with EEP) (Fig. 14d). The six youngest zircons (grains 2-7; outlier grain 1 dismissed) give an $^{206}Pb/^{238}U$ age of 461 ± 2 Ma (± 6 Ma with EEP). Zircons display an oscillatory zoning pattern, Th/U ratios range from 0.2 to 1.1 with a mean of 0.54.

Sample **S1** (15.473E; 47.636N) is a fine-grained, quarzitic sandstone from the basal portion of the Steinbachgraben section well below the first volcanics (Fig. 6). Quartz grains with average grain size of 0.1-0.2 mm are evenly distributed in a fine-grained matrix constituting about 50 % of the volume. In thin section the sandstone is structureless except some tectonically induced pressure solution seams defining a weak foliation. Other detrital components such as feldspar, white mica or lithic components are extremely rare to absent.

A total of 87 zircons were analyzed; one outlier was erased (grain 1) and 11 grains have a discordance between 2 % and 4 %. 7 zircons give Archean ages between ca. 2.55 Ga and 2.65 Ga; 11 give Paleoproterozoic ages between 1.64 Ga and 2.26 Ga; and 14 zircons give Mesoproterozoic ages (1.0 Ga – 1.06 Ga) (see supplementary material, Tab. S1). Neoproterozoic zircons cluster in two $^{206}Pb/^{238}U$ age groups, one at ca. 992 Ma and another at ca. 640 Ma (Fig. 14e). The youngest 6 zircons (youngest outliers dismissed) give a $^{206}Pb/^{238}U$ weighted mean age of ca. 592 Ma.

Sample **S4** (15.444E; 47.624N) is from outside the Steinbachgraben section and corresponds to a level between S1 and S2. It is a coarse-grained, poorly sorted sandstone with a grain size of ca. 1 mm with abundant

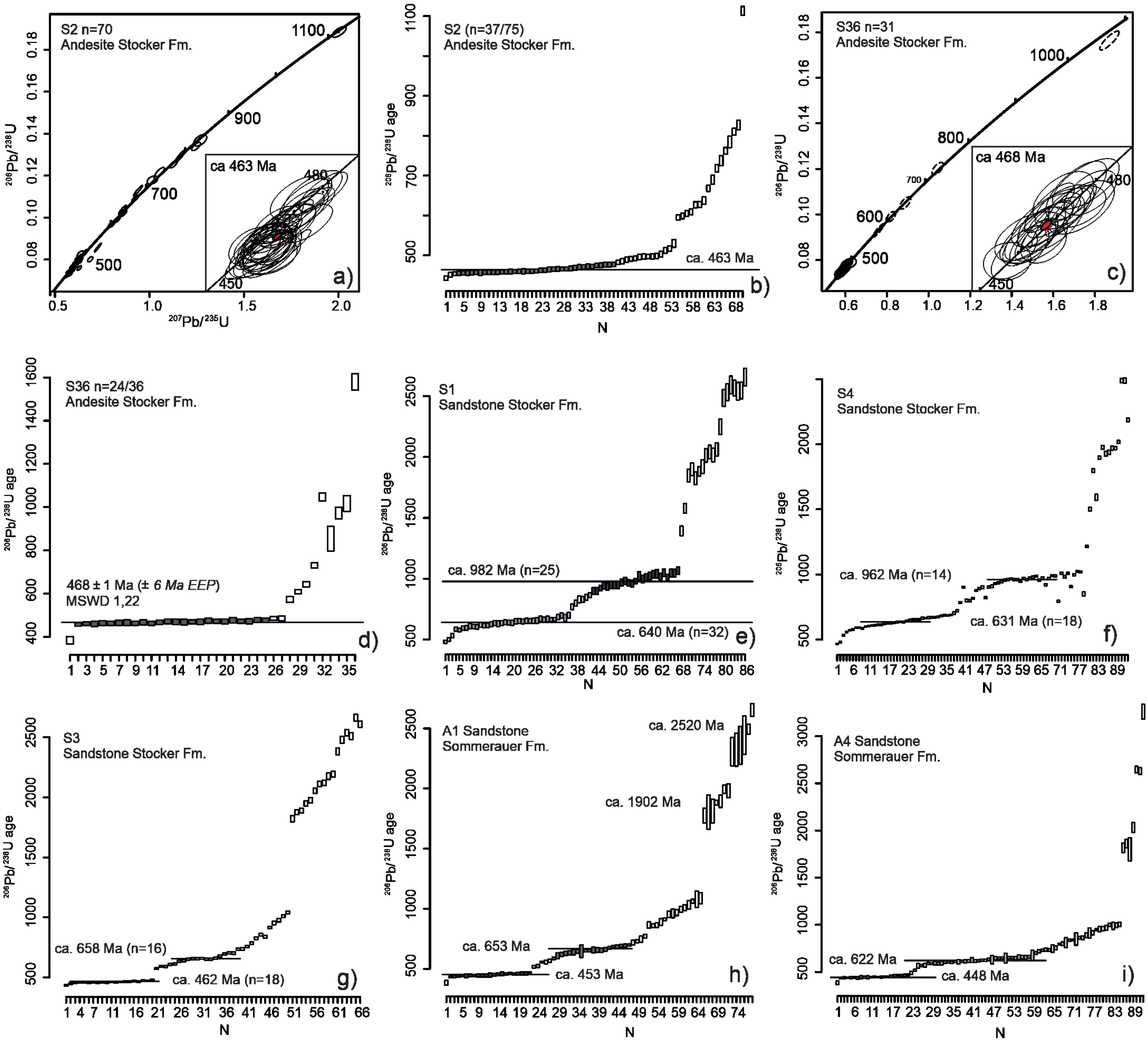

Figure 14: U-Pb zircon Concordia **(a-c)** and $^{206}Pb/^{238}U$ weighted mean age plots of metavolcanics and sandstones from the Stocker Formation **(b-g)** and sandstones from the Sommerauer Formation **(h-i)**. Inserts in (**a**) and (**c**) are Concordia plots and approximate Concordia ages of main age clusters. Uncertainties are 2σ, errors given in Italic characters derived from long-term variance of validation material.

monocrystalline quartz and very rare feldspar grains. Noticeable are fine-grained lithic components, possibly acidic volcanics or chert components. A mild foliation is represented by pressure solution seams.

A total of 94 zircons were measured, 12 of them with more than 2 % discordance were discarded. Four Archean zircons give 2.5 Ga and 2.9 Ga, 10 Paleoproterozoic zircons range between 1.6 and 2.06 Ga. Nine zircons give a Mesoproterozoic age between 1.01 Ga and 1.22 Ga. The majority of zircons is Neoproterozoic with two age groups scattering between 1.05 Ga and 900 Ma (mean $^{206}Pb/^{238}U$ age is ca 962 Ma) and between 700 Ma and 575 Ma (mean $^{206}Pb/^{238}U$ age is ca. 631 Ma) (Fig. 14f). The youngest two zircon grains are Ordovician (470 Ma, 479 Ma). The Th/U ratios in all zircons are > 0.1.

Sample **S3** (15.474E; 47.640N) is a coarse sandstone from the Steinbachgraben section about 20 meters above the andesite sample S2 (Fig. 6). Normal grading can be observed in the field. Components are dominated by monocrystalline quartz, some of which with resorption features. Feldspar grains are rare as are lithic fragments, the latter consisting of andesitic volcanics and phyllites.

A total of 66 zircons were analyzed, 6 of them with more than 2 % discordance were not considered. Five zircons out of the remaining 66 give Archean ages (ca. 2.5 Ga – 2.6 Ga), 11 zircons Paleoproterozoic ages (1.8 Ga – 2.4 Ga), 1 zircon a Mesoproterozoic age (1.07 Ga) and 28 zircons give Neoproterozoic ages between 571 Ma and 999 Ma. The Neoproterozoic to Ordovician zircons are grouped into two clusters (Fig. 14g), one with 16 zircons gives a mean $^{206}Pb/^{238}U$ age of ca. 658 Ma; another with 18 zircons gives ca. 462 Ma. The youngest 6 zircons (except the youngest 437 Ma zircon) give a mean $^{206}Pb/^{238}U$ age of ca. 458 Ma. The Th/U ratios in all zircons are > 0.1.

The summary of zircon ages of Stocker Formation metaclastics is as follows: The basal sandstone (sample S1) contains exclusively Precambrian zircons with the youngest zircon group around 592 Ma. Sample S4, taken from a similar stratigraphic position, shows a similar spectrum but has two zircons with ages of 470 Ma and 479 Ma. This suggests that sandstones were deposited after the early Cambrian, most probably during early Ordovician, but before emplacement of prevalent Middle Ordovician, ca. 460 Ma magmatics of Blasseneck type. The most probable age of sedimentation is the Floian stage which make these sediments approximately time-equivalent to the Gerichtsgraben Formation in the Eisenerz area. The detrital zircon spectrum of sample S3 taken about 20 meters above the andesite sample S2 contains a late Neoproterozoic cluster (658 Ma), similar to the youngest cluster of samples S1 and S4. In addition, a pronounced cluster at 462 Ma is present which is very close to the suggested emplacement age of andesite lavas of sample S2 (463 Ma). Hence a Darriwilian sedimentation age is proposed for sample S3.

4.3.2.3. Metaclastics of the Sommerauer Formation

Sample **A1** (15.363E; 47.650N) is an immature sandstone that contains mainly monocrystalline quartz, rare polycrystalline quartz and up to 10 % lithic components. The latter include sandstone, phyllites and cherty material. Feldspar and white mica are extremely rare. In the outcrop dish structures and convolute bedding can be observed.

A total of 95 zircons were analyzed, 15 of them were dismissed for discordance with more than 2 % or large errors. Out of the remaining 78 zircons 5 zircons give Archean ages (2.5 Ga – 2.7 Ga), 11 zircons Paleoproterozoic ages (1.80 Ga – 2.46 Ga). Seven Mesoproterozoic zircons between 1.01 Ga and 1.10 Ga define together with 8 early Neoproterozoic zircons (908 Ma – 980 Ma) a cluster at 949 ± 2.2 Ma (± 14 Ma with EEP). Out of the 35 Neoproterozoic zircons, the younger group (743 Ma– 555 Ma; n=27) give an array of $^{206}Pb/^{238}U$ ages with a mean age of 653 ± 1 Ma (± 8,5 Ma with EEP). 16 out of 23 Phanerozoic zircons between 436 Ma and 524 Ma give a cluster with 453 ± 1 Ma (± 6 Ma with EEP) (Fig. 14h). The youngest 6 zircons (youngest 3 outlier erased) give a $^{206}Pb/^{238}U$ age of ca. 443 Ma (443 ± 1.5 Ma, ± 6 Ma with EEP).

Sample **A4** (15.352E; 47.648N) is a bedded sandstone with blurred cross stratification. Components include monocrystalline and polycrystalline quartz, some feldspar and lithic components (phyllites, originally probably mud clasts).

A total of 94 zircons were analyzed, 7 of them were dismissed because of discordance > 2 % or large errors. Three Archean zircons give (3.2-2.6 Ga) and two zircons Paleoproterozoic ages (1.83 Ga and 1.84 Ga). Three Mesoproterozoic of 1.01 Ga together with 56 Neoproterozoic zircons (566-980 Ma) give an array of $^{206}Pb/^{238}U$ ages with a cluster (n = 33) at 622 ± 1 Ma (± 8 Ma with EEP). Phanerozoic zircons (n = 18) define a cluster at 448 ± 0.8 Ma (± 6 Ma with EEP) (Fig. 14i). The youngest 6 zircons give a $^{206}Pb/^{238}U$ mean age of 439 Ma.

4.3.2.4. Post -Variscan Cover (Präbichl Formation detrital zircons)

For completeness we include published detrital zircon spectra from Permian sediments (Präbichl Formation) at Präbichl near Eisenerz (Haas et al., 2020). These data and all other U/Pb ages are, for easier assessment, displayed in frequency diagrams (KDE plots, Vermeesch, 2018) (Figs 15-16). Data from these Permo-Mesozoic sediments are considered important because they provide information about the sediment source supplied after the Variscan orogeny. The Precambrian detrital zircon spectrum is similar within all of the studied metaclastics in general (Stocker and Sommerauer Formations), with some Archean to Paleoproterozoic zircons and a Mesoproterozoic age gap. Early Neoproterozoic (“Grenvillian”) ages around 960 Ma are present in the Präbichl Formation, sandstones of the Stocker Formation (S1, S4) and the Sommerauer Formation (A1, A4). Late Neoproterozoic ages around 600 Ma are also comparable to those of samples A1 and A4; an Ordovician peak at ca. 460 Ma documenting erosion of Ordovician magmatics is also present. The major difference is, of course, the very pronounced peak at 356 Ma in the Präbichl sample which documents erosion of an early Variscan orogen in the hinterland.

5. Tectonic structure of the Noric Nappe

The existence of Variscan internal nappes or „Schuppen“ in the Noric Nappe has been taken for granted since the first detailed mapping of the study area (Cornelius; 1936, 1952). Variscan nappes have also been described from other well-studied areas of the Greywacke Zone like the Eisenerz Mountains (e.g., Schönlaub, 1982) and Kitzbühel (e.g., Heinisch et al., 2015). Eo-Alpine tectonics, most probably of Lower Cretaceous age is inferred from Permo-Mesozoic sediments interposed with Paleozoic sequences (basement-cover repetition) and scattered cooling ages (Ratschbacher, 1986; Neubauer et al., 1994; Dallmeyer et al., 1998; Schuster and Nowotny, 2015). In the study area the tectonic boundaries of the Tirolic-Noric Nappe System are certainly of eo-Alpine age. The tectonic base of the Noric Nappe is underlain by Permian sediments of the Silbersberg Nappe and occasionally by tectonic slices of magnesite (Veitsch Nappe) and high-grade metamorphic Kaintaleck slices. On the top, the Präbichl Formation is only partially resting undisturbed on its Lower Paleozoic basement. In many cases Permian sediments are incorporated into thrust tectonics, e.g., along the Rotsohl Thrust (Figs 3-4). The Tirolic-Noric Nappe System is overthrusted by the Juvavic Mürzalpen Nappe with Permian gabbros and rauwacke exposed

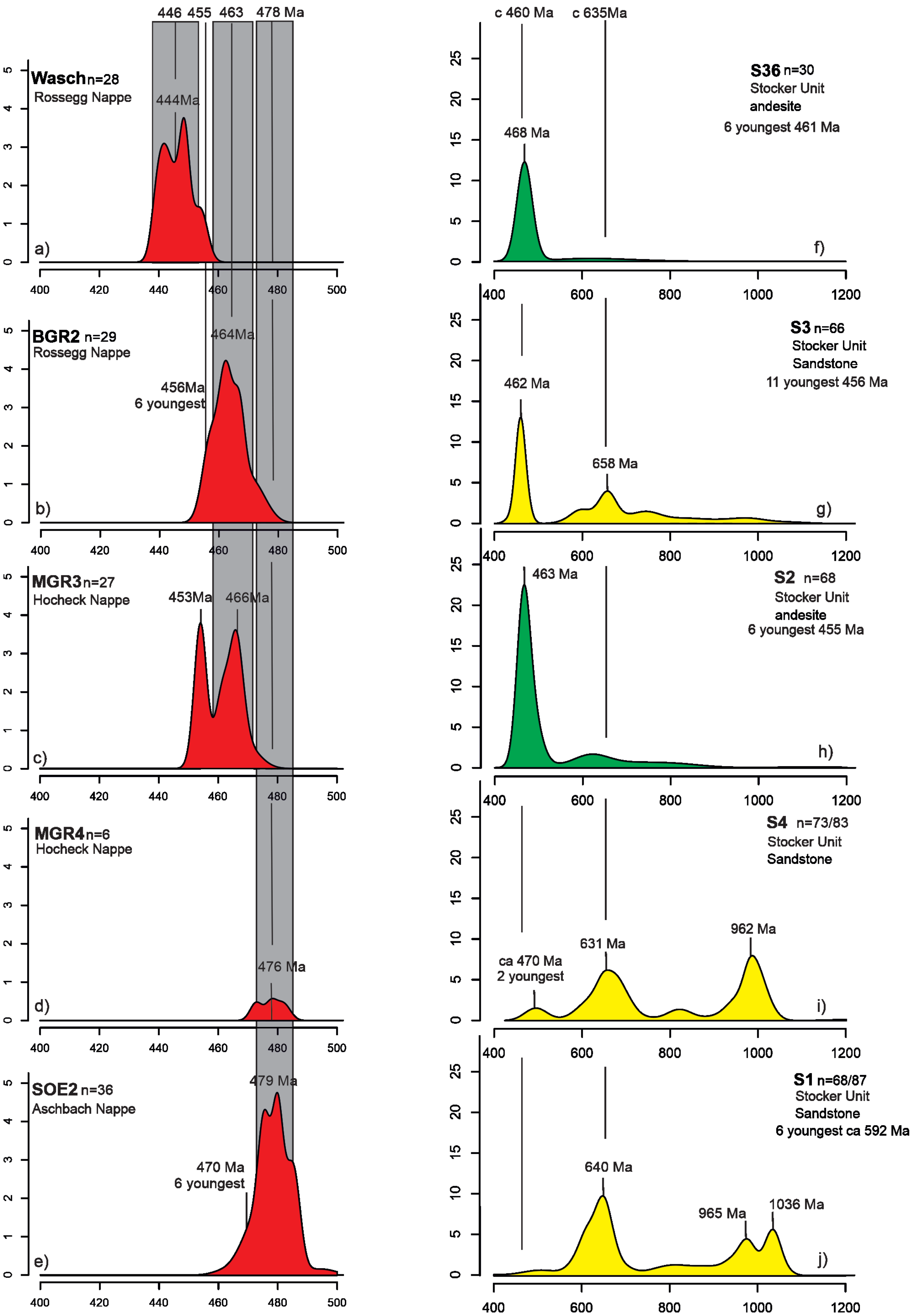

Figure 15: Kernel density estimation graphs (KDE-Plots; Vermeesch, 2012). Blasseneck Porphyroids **(a-e)** are arranged by age groups and display pulses of zircon formation at ca. 478 Ma, 462, 455 Ma and 446 Ma. Youngest zircon ages closely date age of volcanic eruption. Ages from Stocker Formation **(f-j)** are arranged from stratigraphic base **(j)** to top **(f)** and include andesite (green) and sandstone (yellow). Cut-off is 1.2 Ga. Note increase of Ordovician source material with time and decrease of Neoproterozoic detritus. Age of sedimentation of sandstone S3 is considered close to emplacement of andesites (S2, S36).

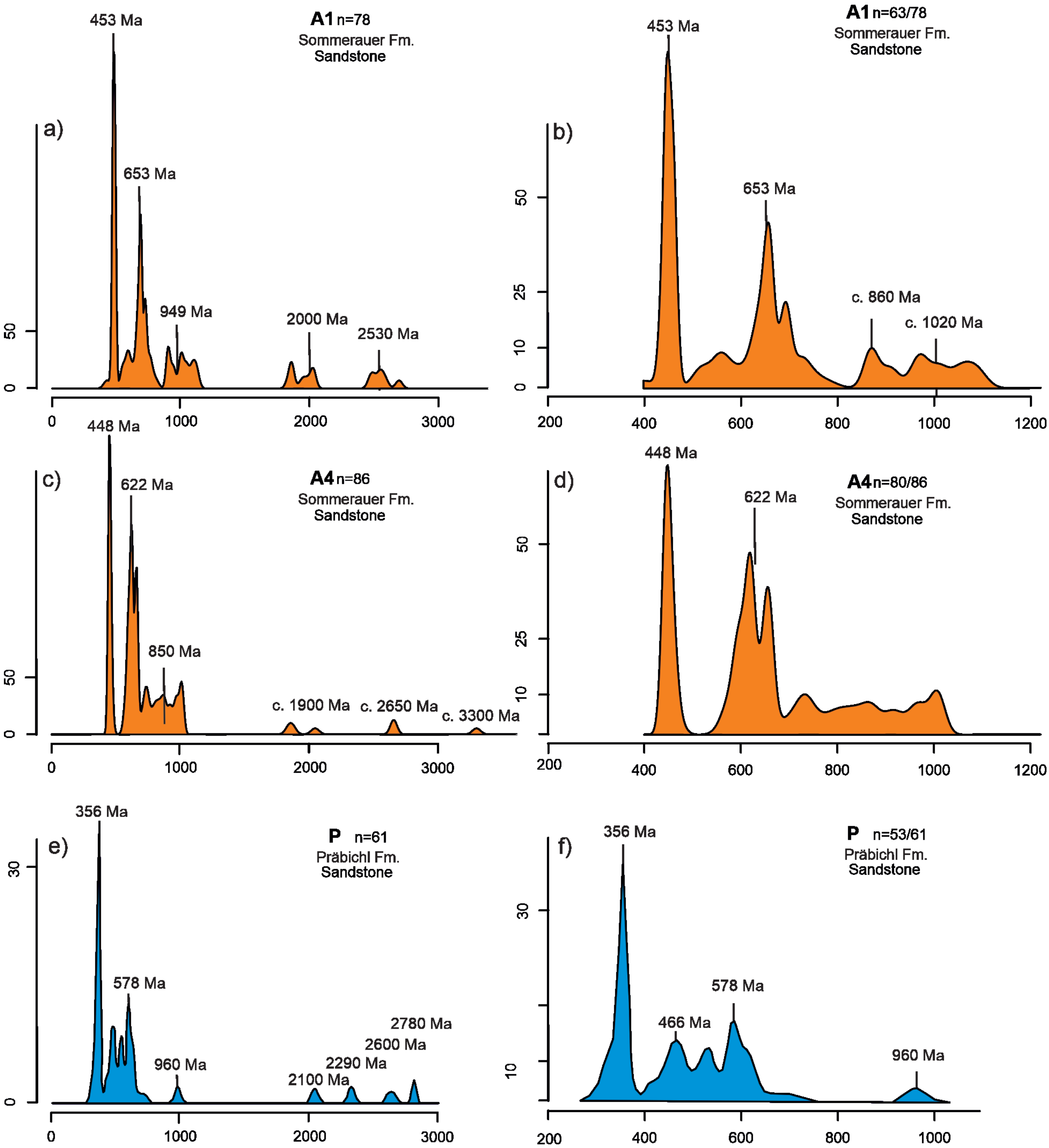

Figure 16: Kernel density estimation graphs (KDE-Plots) from the Sommerauer Formation **(a-d**; orange) and the Präbichl Formation **(e-f**: blue**)**. Cut-off is 3.0 Ga, 1.2 Ga and 1.0 Ga. Youngest peak in Sommerauer Formation samples (A1, A4) is 455 Ma and 448 Ma which is close to the ages obtained from the younger Blasseneck Porphyroid in sample Wasch (ca. 444 Ma) and the younger group of sample MGR3 (ca. 453 Ma). The post-Variscan sediments of the Präbichl Formation **(e-f)** sampled Blasseneck Porphyroid and, as seen in the most pronounced peak, an early Variscan (ca. 356 Ma) magmatic hinterland (data from Haas et al., 2020).

along the thrust contact. By combining the zircon age data, published biostratigraphic data and mapping, four nappes can be distinguished within the Tirolic-Noric Nappe System at Veitsch area. These are from south to north the Hocheck, Rossegg, Steinbach and Aschbach Nappes (Fig. 3).

5.1 Hocheck Nappe

The Hocheck Nappe consists mainly of Blasseneck Porphyroid and builds the steeply dipping southern rim of the Noric Nappe in the study area. The Noric Thrust separates it from the underlying tectonic units (Silbersberg Nappe, Kaintaleck slices, and Veitsch Nappe).

In the northeast, near Neuberg, phyllites and limestone marbles of Rad Formation and Kaiserstein Formation, respectively, occur on top of the Blasseneck Porphyroid in a mélange-like fashion, the irregular arrangement (imbrication of slices) is caused by the overriding Rossegg Nappe. In the very southwest of the study area, phyllites and marbles of the Gerichtsgraben Formation as well as Polster Quartzite and phyllites of the Rad Formation belong also to this nappe.

The Hocheck Nappe is, however, not limited to the southern rim of the Noric Nappe. West of the Almweg Fault, Blasseneck Porphyroid, limestone marbles of Kaiserstein Formation, remnants of Polster Quartzite and phyllites of the Rad Formation crop out beneath Rossegg and Steinbach Nappes and are thrust upon inverted Permian Präbichl Formation (Fig. 4). Thrusting is therefore of eo-Alpine age. East of the Almweg Fault and south of Brunnalm (south of Hohe Veitsch), flat-lying marbles of the Kaiserstein Formation appear as tectonic windows below the steeply dipping Stocker Formation in Pammer- and Brunnbauergraben, respectively (Figs 2-S1). The Hocheck Nappe is the only nappe that continues beyond the study area to the northeast (GK50 Sheet 104 Mürzzuschlag) and to the southwest (GK50 Sheet 102 Aflenz).

5.2 Rossegg Nappe

On top of Hocheck Nappe and below Steinbach Nappe lies the Rossegg Nappe, comprising Blasseneck Porphyroid, Rad Formation and Kaskögerl Formation in an obviously undisturbed succession (Figs 2-3). The Rossegg Nappe is the largest of the internal nappes. West of Neuberg, Blasseneck Porphyroid rests on younger Rad and Kaiserstein Formations of the Hocheck Nappe. The thrust plane between the two nappes is gently northwest dipping, parallel to the main foliation in the Blasseneck Porphyroid (Nievoll, 2015). Further to the southwest the base of Rossegg Nappe is marked by isolated slices of calcitic marble (Kaiserstein Formation) within Blasseneck Porphyroid. For the larger part, however, Blasseneck Porphyroid of the Rossegg Nappe is resting directly on Blasseneck Porphyroid of the Hocheck Nappe and the exact position of the boundary between the two internal nappes is hypothetical (Nievoll, 2015). West of the Almweg Fault, in Hinterhofgraben, slices of calcitic marble of Kaiserstein Formation are tapering again the tectonic boundary to the underlying Hocheck Nappe over more than 1 km. South of Hohe Veitsch and northwest of Rauschkogel, the Rossegg Nappe is tectonically overlain by the Steinbach Nappe whereas south of Rauschkogel the Präbichl Formation rests transgressively on it (supplementary material, Fig. S1,). Here, the Rossegg Nappe is overthrusted by the Juvavic Rauschkogel klippe.

In the northeastern part of the study area the minimum amount of displacement of the Rossegg Nappe upon the Hocheck Nappe is, from profile restoration, at least 1.25 km. Overall shortening of the Noric Nappe in this sector has been calculated as 67 % (Haller, 2016). Here, north of Neuberg (Fig. 3), the overlying Präbichl Formation and the Triassic carbonates of the Juvavic Mürzalpen Nappe are tilted into vertical position, proving eo-Alpine age of thrusting.

5.3 Steinbach Nappe

The Steinbach Nappe, exposed south of Hohe Veitsch and northwest of Rauschkogel, comprises a succession of the Stocker Formation, the Kaskögerl Formation and rare occurrences of the Eisenerz Formation. These are transgressively overlain by the Präbichl Formation (Fig. 5). Below of the Steinbach Nappe, another trail of Kaskögerl Formation is exposed that belongs to the Rossegg Nappe. South and southwest of Rauschkogel, metasediments of the Rad and Kaskögerl Formations of the Rossegg Nappe are transgressively overlain by the Präbichl Formation whereas west of Rauschkogel and south of Hohe Veitsch the Präbichl Formation rests transgressively on metasediments of the Steinbach Nappe (Fig. 2). Permian Präbichl Formation on top of the Rossegg and Steinbach Nappes, respectively, suggest a pre-Alpine, i.e. Variscan tectonic contact between these two nappes.

The displacement of the Steinbach Nappe upon the Rossegg Nappe cannot be quantified from profile restoration. The pronounced differences in magmatic and sedimentary facies between the Rossegg and Steinbach Nappes lead us to argue for a considerable displacement during Variscan times, in the order of tens of kilometers.

5.4 Aschbach Nappe

This nappe consists of the Blasseneck Porphyroid of the Sommereck and metaclastics of the Sommerauer Formation. In the north, the Blasseneck Porphyroid is thrusted upon the Präbichl Formation while towards the south the metasediments of the Sommerauer Formation are covered by the Präbichl Formation. A major thrust (Rotsohl Thrust: Figs 2-3) that can be traced over a length of 2 km separates the metaclastics of the Präbichl and Werfen Formations (Aschbach Nappe) from early Paleozoic rocks the Hocheck Nappe. The zircon age of sample SOE2 (ca. 478 Ma) excludes a direct connection with the younger Blasseneck Porphyroid of the Hocheck and Rossegg Nappes, like assumed in a previous paper (Nievoll, 2015).

5.5 Retro-deformation of internal nappe tectonics

Cross sections were drawn to the west of the Almweg Fault where all four internal nappes are exposed (Fig. 4). A semi-quantitative profile restoration is depicted in Figure 17. Our balancing of the profile through the Rauschkogel gives an eo-Alpine shortening of ca. 36 %, similar to previous calculations of 40 % shortening or 18 km nappe displacement (Haller, 2016). These data represent, however, only minimum shortening and displacement, for the following reasons: (a) only discrete structures like thrusts or faults are considered but no ductile deformation; (b) the cut-off points for the Aschbach, Steinbach and Rauschkogel Nappes cannot

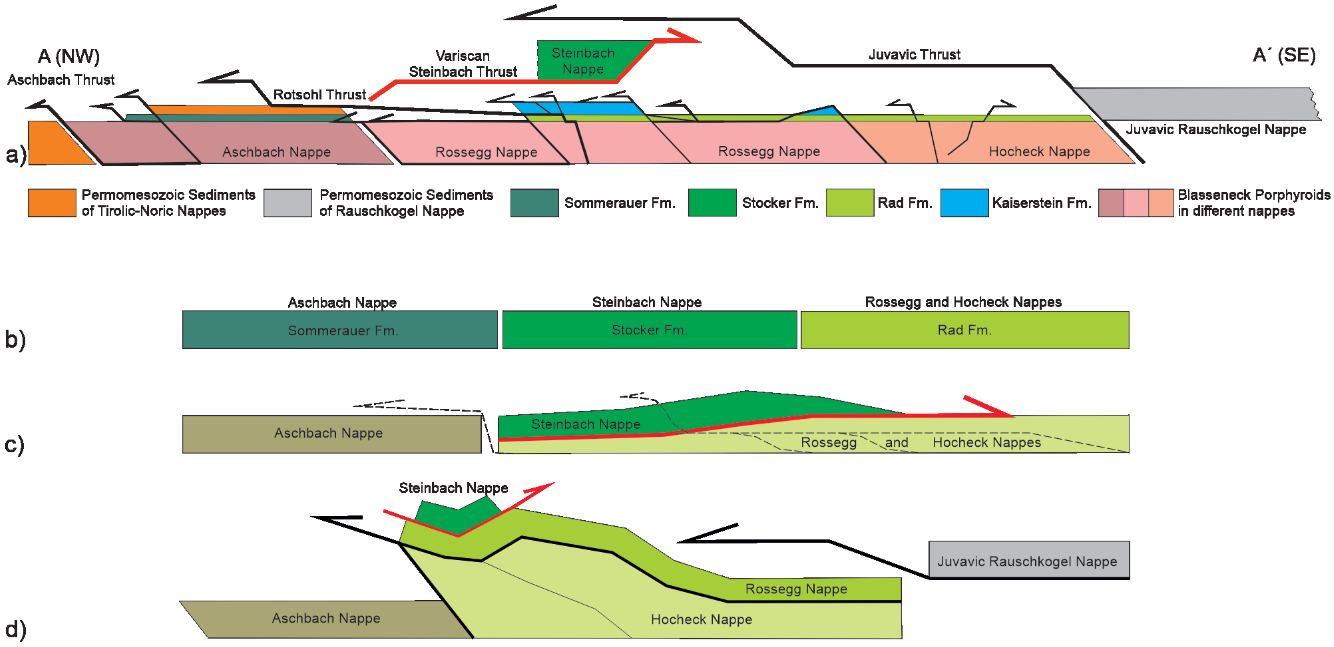

Figure 17: (a) Semiquantitative retro-deformation of the profile through Rauschkogel Klippe. Variscan thrust in red, eo-Alpine thrusts in black. **(b-d)** Simplified tectonic evolution with forward modelling steps from the original, lower Paleozoic distribution of nappes and facies domains **(b)**; Variscan thrusting (red half arrow; main future Alpine thrust are stippled black) **(c)**; to final nappe assembly with main eo-Alpine thrusts (black half arrows) **(d)**.

be sufficiently defined and hence the spatial origin of these nappes remains unknown; (c) Variscan thrusting has not been considered. The aim of the restoration was primarily to derive a plausible scenario for explaining the recent configuration of nappes and, thus, the original, spatial distribution of facies domains (Fig. 17). The arrangement of nappes suggests, in recent coordinates, the Aschbach Nappe in the north and lowermost position, the Steinbach Nappe in the middle and the Rossegg and Hocheck Nappes in the south and highest position. During Variscan times the Steinbach Nappe was emplaced over the area of the future Rossegg and Hocheck Nappes. Eo-Alpine tectonics disrupted this area and stacked the Rossegg Nappe over the Hocheck Nappe, the former carrying the Steinbach Nappe in a piggy-back fashion. Finally, the entire nappe pile was thrusted over the Aschbach Nappe (Figs 17 b-d).

6. Discussion

6.1 Magma generation, eruption and sediment deposition

Even when large errors as derived from EEP are considered, our LA-MC-ICP-MS U-Pb zircon ages of the Blasseneck Porphyroid form clusters at ca. 478 Ma, 465-460 Ma and 454-446 Ma. Taking the youngest zircon ages per cluster as indicators for the age of eruption, pulses may have occurred at 470 Ma, 453-456 Ma and ca. 440 Ma (Figs 15-18). Given the relatively small number of samples, the error range of the calculations and the inherent limitations of the analytical method, an evaluation whether these clusters really reflect individual eruptive pulses is not straightforward. Nevertheless, in a regional overview of low-grade metamorphic pre-Variscan volcanics and metasediments, Early, Middle as well as Late Ordovician volcanic activities are plausible. Zircons from the Western Greywacke Zone analyzed by the same method yielded ages between 471 and 461 Ma with clusters at 471-469 Ma, 465-464 Ma and 462-461 Ma (Blatt, 2013). South Alpine LA-ICP-MS U-Pb zircon ages of felsic volcanic to subvolcanic rocks of the Val Visdende Formation are clustered at 474-472 Ma and 454-452 Ma (Arboit et al., 2019) while earlier U-Pb TIMS and Pb-Pb evaporation zircon analyses suggested volcanic activities at ca. 485 Ma and 479 Ma (Meli and Klötzli, 2001) and the first U-Pb zircon analyses of North and South Alpine rhyodacitic porphyroids resulted in ages of 467-463 Ma (Söllner et al., 1991; 1997).

Combining information from age data of Blasseneck Porphyroids with those derived from the Stocker and Sommerauer Formations suggests the existence of individual magmatic pulses, interrupted by phases of sedimentation (Fig. 18). Sample S1 from the Stocker Formation was deposited before onset of Ordovician magmatism as no such zircons occur in that sample (Fig. 18, compare with KDE plots – Fig. 15). By ca. 470 Ma - 480 Ma a first pulse of magmatism occurred (MGR4, SOE2, S36). The main phase of dacitic magmatism occurred at ca. 460 Ma - 465 Ma (MGR3, BGR2). The zircon age pattern of S3 sandstones includes a pronounced peak at ca. 460 Ma but no younger ones. Thus, we interpret S3 sandstone deposition approximately coeval with emplacement of the andesite S2 and the dacites MGR3 and BGR2. Later than ca. 455 Ma the Sommerauer sandstone samples A1 and A4 were deposited that contain detrital zircon peaks at 455 Ma and 448 Ma, approximately coeval with the youngest magmatic pulse at ca. 454 Ma (MGR3

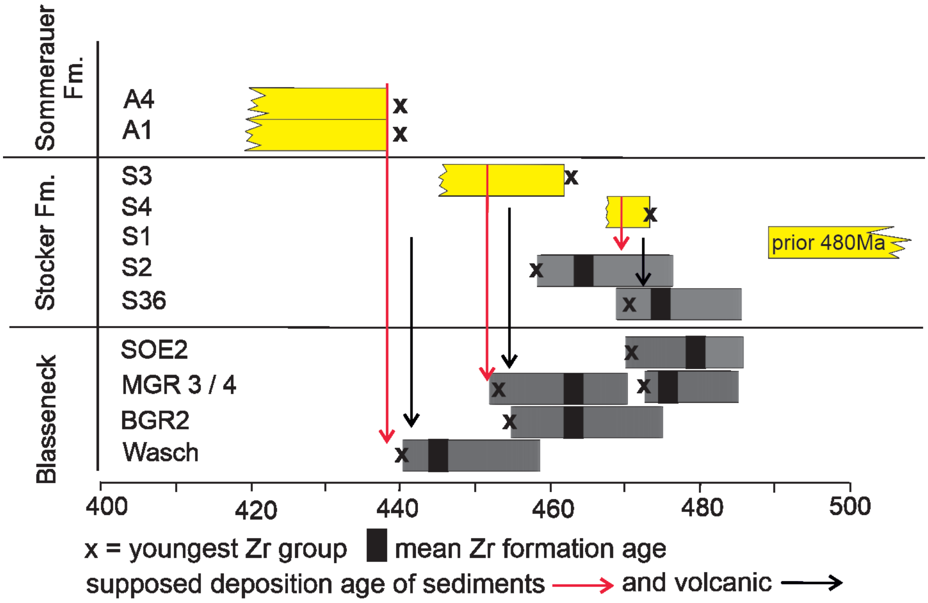

Figure 18: Summary of Ordovician and Silurian magmatic and sedimentary pulses. Grey is scatter of zircon ages derived from Blasseneck Porphyroids and Stocker Formation metavolcanics with black bar giving mean ages. Yellow bars give estimated age range of deposition of sediments. Bold **x** show youngest zircon groups found in magmatics and youngest peaks in detrital zircon age spectra of sediments (compare with Figures 12-14). Youngest 2-3 zircons have been omitted for possible outliers and / or lead loss and the mean of the next-older 4-6 zircons was taken to define the "youngest age group". Black arrows are suggested time of magma eruption, red arrows suggested time of sediment deposition.

younger age group). Young ages of sample WASCH (ca. 446 Ma) are unique. Nevertheless, as similar ages are found in the detrital spectrum of samples A1 and A4 from the Sommerauer Formation (453 Ma - 448 Ma; Fig. 16) a young, Katian to Hirnantian, magmatic pulse seems plausible.

Another open question concerning the volcanics is the large scattering of U/Pb zircon ages along the Concordia, and, in case of sample MGR3, the apparent presence of two concordant age groups at ca. 466 Ma and 453 Ma. Being an effusive rock (dacitic ignimbrite) the eruption is a short time process but the supply of zircons to be erupted is obviously not. A probable analogue to explain this scenario of successive eruptions was described from the Jemez Mountains volcanic field at Rio Grande Rift, Mexico (Wu et al., 2021). The authors describe a succession of individual eruptions over a 10 Myr time span, zircon ages of single eruptions spread over ca. 2 Ma. They explain this scenario by multiple intrusions of host granitoids at 40-10 kilometers depth that fed volcanic eruptions. Those in turn sampled on their way different aged "inherited" zircons. In our case, magmatism continued over a period of at least 40 Myr with an age scatter of individual magmatics up to 20 Myr. Although time intervals are much larger than described from the Jemez Mountains volcanic field, the principal mechanism to explain that age scattering seems applicable.

6.2 Facies distribution

Retro-deforming of the tectonics of internal Noric nappes leads to the following picture of the sedimentary facies distribution: In today´s southeast, on several hundred meters thick Middle Ordovician Blasseneck Porphyroid fine-grained metaclastics of the Rad Formation were deposited in a shallow sea during Late Ordovician and Silurian. As mentioned in chapter 3.1., evidence for erosion or reworking of the Blasseneck Porphyroid is scarce in the study area. Uniform phyllites do not really lend for reconstruction of depositional environment. Although sandy layers are absent, diffuse layering in the mm-scale bears some resemblance to graded rhythmites, i.e. storm-sand layers embedded in shelf mud (Reineck and Singh, 1972). The fossils in the middle part of the Rad Formation may also have been deposited in a shallow shelf environment. Based on $^{40}Ar/^{39}Ar$ white mica ages of detrital material, a metamorphic, Pan-African hinterland was proposed for the Rad Formation (Handler et al., 1997). The Devonian is represented by calcitic marbles (Kaiserstein Formation) and banded limestones to phyllitic limestones accompanied by siliceous phyllites (Kaskögerl Formation), the latter probably deposited in a pelagic basinal environment.

To the northwest, during Early and Middle Ordovician a slope environment and/or marginal basin prevailed where phyllites, sandstones, volcanics and volcaniclastics were deposited. The Middle Ordovician volcanics and volcaniclastics of the Stocker Formation resemble marginal basin sediments of the present Aegean volcanic arc in the eastern Mediterranean with, e.g., lava flows and debris avalanche flows interbedded with shales (Anagnastopoulos and Anastasakis, 2020). The breccia layer of the Kaiblinggraben may have resulted from a volcanigenic debris flow. The upper part of the Stocker Formation and the Kaskögerl Formation on top of it,

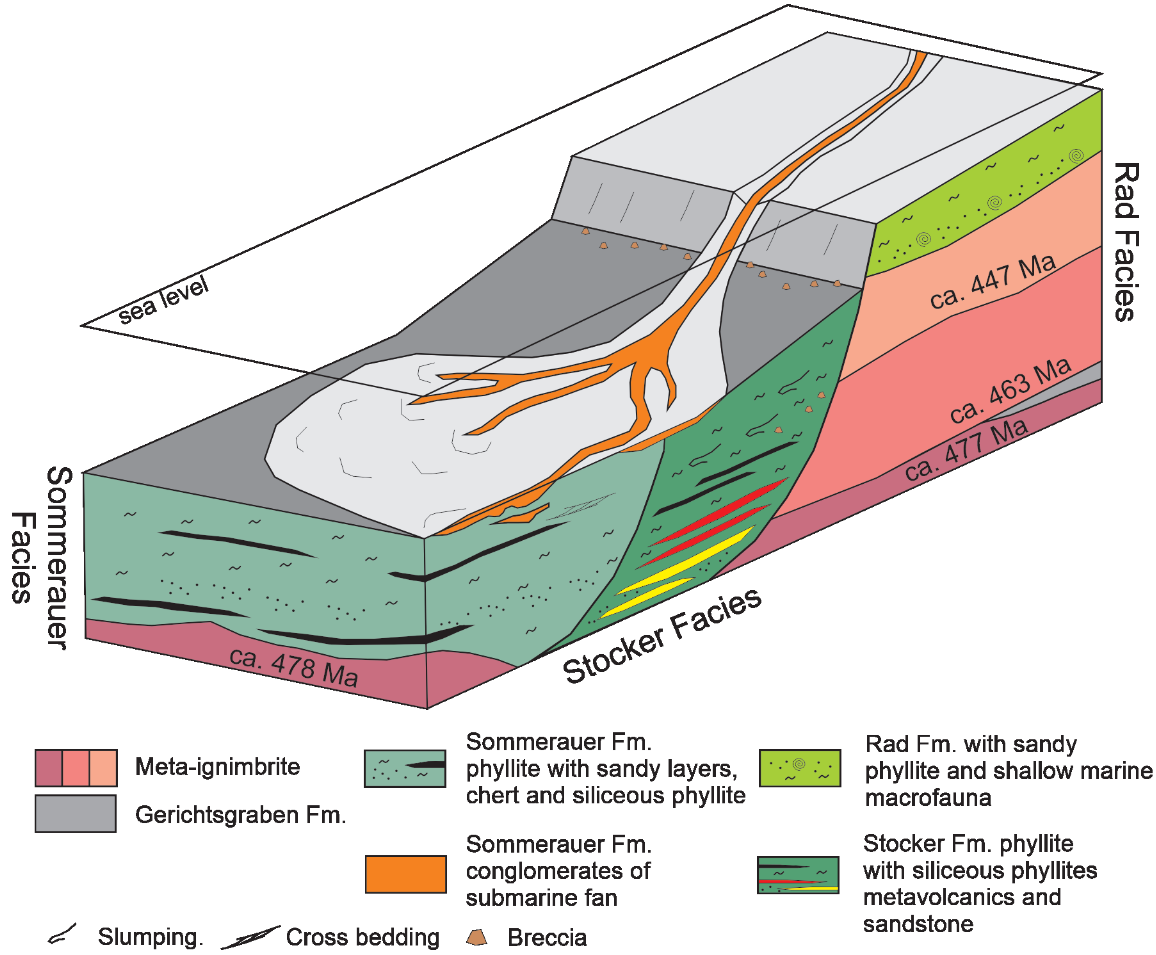

Figure 19: Model sketch showing the Silurian (ca. 430 Ma) arrangement of facies domains on a sloping continental margin with Rad Facies in the southeast and Sommerauer Facies in the present days' northwest. By that time the youngest pulse of Blasseneck Porphyroids was partly close to surface and ready to deliver detritus to the submarine fan represented by the Sommerauer Formation.

deposited during Silurian and Devonian, can be well compared with the corresponding lithologies and sedimentary facies to the southeast.

In the northwest, Early Ordovician Blasseneck Porphyroid of <300 m thickness is overlain by deep-water sediments, as indicated by the metaturbidites of the Sommerauer Formation. These sediments were not deposited before Late Ordovician or even Llandovery, as constrained by the detrital zircon ages derived from that sediments (Fig. 18). The apparent mismatch of subaerally erupted ignimbrites and deep-water sediments on top of it can be reconciled by considering this time gap. Around the Ordovician-Silurian boundary, approximately 30 million years after emplacement, the Blasseneck Porphyroid of the Sommereck was completely drowned beyond the shelf edge. Structures distinctive for tempestites of an outer shelf of ancient epeiric seas, like thin-bedded sandstones displaying hummocky cross stratification or abundant lenticular, wave ripple cross-laminated sandstones (e.g., Grundvåg et al., 2021) are absent in the Sommerauer Formation. The sedimentary structures are therefore considered typical for turbidites deposited in the proximal lobe and in outer, distal parts of a submarine fan, respectively (Fig. 19). Whether the turbiditic sedimentation persisted throughout the Silurian or continued even into the Devonian is not known. Note that in the Glemmtal Unit of the Western Greywacke Zone, turbiditic sedimentation has prevailed over some 140 million years, from early Ordovician to Mississippian (Heinisch et al., 2015).

6.3 Regional comparison

In the Kitzbühel area as well as in the Eisenerz Mountains, Blasseneck Porphyroid is largely controlling the subsequent sedimentary environment. At Kitzbühel, on thick volcanic "platforms" Silurian and Devonian shallow-water limestones and dolomites of the Wildseeloder Unit are deposited (Heinisch et al., 2015) and a similar succession is exposed at Eisenerz (Schönlaub, 1982). The Veitsch area does not follow this pattern, with several hundred meters of Blasseneck Porphyroid overlain by several hundred meters of clastic shallow-water meta-sediments (Rad Formation) or deep-water meta-turbidites (Sommerauer Formation). The absence of "volcanic platforms" may be explained by caldera-like structures where most of the erupted ignimbrite is redeposited (e.g., Best et al., 2016). It must be stressed that no greenschists or other types of basic volcanics are found in the Stocker Formation; the Stocker Formation bears thus little resemblance with the lithologies of the Lange Teichen – Wildfeld section in the Eisenerz Mountains (Schönlaub, 1982). There, as well as in the Kitzbühel area, greenschists have been deposited as basalts, pyroclastics, basic lapilli and ash tuffs from subaeral and submarine volcanoes in an overall shallow water environment (<500 m) near a passive continental margin. Geochemical data typical for ocean island basalts support the petrographic interpretation (Schlaegel-Blaut, 1990).

From the Eisenerz Mountains or other parts of the Eastern Greywacke Zone no meta-turbidites have yet been described although in the Wildfeld Nappe metaclastics are predominant (Schönlaub, 1982). Meta-turbidites are, however, well-known from the Western Greywacke Zone. In the Glemmtal Unit they have been deposited from Lower Ordovician on to Mississippian and host basic volcanics, gabbros and diorites (Heinisch et al., 2015). Neither in the Sommerauer Formation nor in the Stocker Formation are basic rocks exposed; not even lithoclasts or grains of basic composition are encountered in the various metaclastics. Another difference to the meta-turbidites of the Western Greywacke Zone is the provenance of the clastic material. Here, the detrital material is derived mainly from a metamorphic-magmatic, cratonic hinterland (Heinisch et al., 2015). The Sommerauer Formation, on the contrary, seems to have been sourced mainly from the Blasseneck Porphyroid.

6.4 Paleogeographic position of the Noric Group

Recent papers dealing with the early Paleozoic evolution of Alpine domains generally agree that the future Austroalpine was located on the northern margin of Gondwana (Haas et al., 2020; Neubauer et al., 2020; Burda et al., 2021). During the late Neoproterozoic and early Cambrian this margin was covered by sandstones of the so-called Gondwana superfan (Meinhold et al., 2013). Zircons of sample S1 of the Stocker Formation with a pronounced Pan-African peak around 630 Ma – 640 Ma could well be derived from such sandstones. By ca. 480 Ma an orogenic phase, sometimes referred to as Ceneric orogeny (Zurbriggen, 2017; Burda et al. 2021), developed along the eastern north Gondwana margin, associated with a southward dipping subduction zone beneath continental Gondwana. Zircons of samples SOE2 and MGR4 (ca. 480 Ma - 475 Ma) are attributed to magmatics generated in such a tectonic context. At around 463 Ma, magma generation reached its climax with deposition of the main part of the dacitic Blasseneck Porphyroid. These porphyroids were generated in an extension domain in the back of the retreating Prototethys subduction zone and are alternating with passive margin sediments. Zircon ages from the Sommerauer Formation (samples A1 and A4) but also from sample WASCH indicate that magmatic activity continued throughout the Late Ordovician. Turbidites of the Sommerauer Formation indicate that after ca. 440 Ma a deep-sea environment had evolved in this part of the Gondwana margin.

7. Conclusion

U/Pb zircon ages of Blasseneck Porphyroids cover the entire Ordovician between ca. 479 Ma to 444 Ma and represent calc-alkaline rhyolitic to dacitic volcanics. Coeval with the main phase of dacitic volcanism andesites and rhyolites of the Stocker Formation erupted. Sandstone of the Stocker Formation are partly older or contemporaneous with Middle Ordovician magmatism. Zircons from meta-turbidites of the Sommerauer Formation were deposited later than ca. 453 Ma – 448 Ma. The source of clastic sediments was the northern Gondwana continental margin (ca. 640 Ma) and Ordovician volcanics dated 462 Ma – 448 Ma.

The distribution of zircon ages allows distinction of several internal tectonic nappes within the Noric Nappe that were assembled during eo-Alpine but also Variscan events. Profile restoration of these internal nappes leads to an arrangement of Ordovician to Devonian facies domains with shallow marine environment in the todays southeast. An intermediate sloping continental margin occurs further to the northwest and a deep-sea environment in the northwest.

Acknowledgements

We acknowledge reviews by Hugo Ortner, Franz Neubauer and Gerd Rantitsch which greatly improved the manuscript. Geologische Bundesanstalt (GBA) in Vienna supported mapping on GK50 Blatt 103 Kindberg throughout the years and discussions with GBA geologists Ralf Schuster, Gerhard Bryda and Gerhard Mandl are very appreciated. Topographic maps were made available by the Bundesamt für Eich- und Vermessungswesen (BEV: data.bev.gv.at). Roman Pongratz (Wernersdorf) cut many "greywacke" specimens, Martin Lohner (Veitsch) provided access to the XRF device at RHI Magnesita´s Veitsch plant, and Gabriel Nievoll (Montanuniversität Leoben) prepared additional thin sections of meta-turbidites from Aschbach. Isabelle Haas and Etienne Skrzypek are acknowledged for help in zircon preparation and dating.

References

Anagnastopoulos, V.K., Anastasakis, G., 2020. Volcanogenic mass flow deposits and seafloor diapirism following the largest insular Quaternary eruption of the eastern Mediterranean at Nisyros island, Aegean volcanic arc. Marine Geology, 425, 106185. https://doi.org/10.1016/j.margeo.2020.106185

Arboit, F., Chew, D., Visoná, D., Massironi, M., Sciascia, F., Benedetti, G., Rodani, S., 2019. The geodynamic evolution of the Italian South Alpine basement from the Ediacaran to the Carboniferous: Was the South Alpine basement terrane part of the peri-Gondwana arc-forming terranes? Gondwana Research, 65, 17–30. https://doi.org/10.1016/j.gr.2018.08.005

Baker, M.L., Baas, J.H., 2020. Mixed sand-mud bedforms produced by transient turbulent flows in the fringe of submarine fans: Indicators of flow transformation. Sedimentology, 67, 2645 – 2671. https://doi.org/10.1111/sed.12714

Best, M.G., Christiansen, E.H., de Silva, S., Lipman, P.W., 2016. Slab-rollback ignimbrite flareups in the southern Great Basin and other Cenozoic American arcs: A distinct style of arc volcanism. Geosphere, 12, 1097–1135. https://doi.org/10.1130/GES01285.1

Black, L.P., Gulson, B.L., 1978. The age of the mud tank carbonatite, Strangways Range, Northern Territory. BMR Journal of Australian Geology and Geophysics, 3, 227–232.

Blatt, A., 2013. Geochronologische Datierungen in der Grauwackenzone Tirols. Hallesches Jahrbuch der Geowissenschaften, Beiheft 29, 3–59.

Brooks, H.L., Hodgson, D.M., Brunt, R.L., Peakall, J., Hofstra, M., Flint, S.S., 2018. Deep-water channel-lobe transition zone dynamics: Processes and depositional architecture, an example from the Karoo Basin, South Africa. GSA Bulletin, 130, 1723–1746. https://doi.org/10.1130/B31714.1

Bryda, G., Husen van, D., Kreuss, O., Koukal, V., Moser, M., Pavlik, W., Schönlaub, H.P., Wagreich, M., 2013. Erläuterungen zu Blatt 101 Eisenerz. Geologische Bundesanstalt, 223 pp.

Burda, J., Klötzli, U., Majka, J., Chew, D., Li, Q., Liu, Y., Gawęda, A., Wiedenbeck, M., 2021. Tracing proto-Rheic - Qaidam Ocean vestiges into the Western Tatra Mountains and implications for the Palaeozoic palaeogeography of Central Europe. Gondwana Research, 91, 188–204. https://doi.org/10.1016/j.gr.2020.12.016

Butler, R.W.H., Eggenhuisen, J.T., Haughton, P., McCaffrey, W.D., 2016. Interpreting syndepositional sediment remobilization and deformation beneath submarine gravity flows; a kinematic boundary layer approach. Journal of the Geological Society, 173, 46–58. https://doi:10.1144/jgs2014-150

Chappell, B.W., White, A.J.R., 2001. Two contrasting granite types: 25 years later. Australian Journal of Earth Sciences, 48, 489–499. https://doi.org/10.1046/j.1440-0952.2001.00882.x

Cornelius, H.P., 1936. Geologische Spezialkarte des Bundesstaates Österreich 1:75.000, Blatt Mürzzuschlag. Geologische Bundesanstalt, Wien.

Cornelius, H.P., 1939. Zur Schichtfolge und Tektonik der Mürztaler Kalkalpen. Jahrbuch der Reichsstelle für Bodenforschung, Zweigstelle Wien, 89, 27–175.

Cornelius, H.P., 1952. Gesteine und Tektonik im Ostabschnitt der nordalpinen Grauwackenzone, vom Alpenostrand bis zum Aflenzer Becken. Mitteilungen der Geologischen Gesellschaft Wien, 42/43 (1949-1950), 1–234.

Dallmeyer, R.D., Handler, R., Neubauer, F., Fritz, H., 1998. Sequence of thrusting within a thick-skinned tectonic wedge: Evidence from $^{40}Ar/^{39}Ar$ ages from the Austroalpine nappe complex of the Eastern Alps. Journal of Geology, 106, 71–86. https://doi.org/10.1086/516008

Dallmeyer, R.D., Neubauer, F., Handler, R., Fritz, H., Müller, W., Pana, D., Putis, M., 1996. Tectonothermal evolution of the internal Alps and Carpathians: $^{40}Ar/^{39}Ar$ mineral and whole rock data. Eclogae Geologicae Helvetiae, 89, 203–277. https://doi.org/10.1016/S0040-1951(98)00006-7

Ebner, F., 1974. Bericht 1973 über stratigraphische Untersuchungen in der Steirischen Grauwackenzone (Raum Veitsch-Aflenz). Verhandlungen der Geologischen Bundesanstalt, 1974, A116–A118.

Flajs, G., Schönlaub, H.P., 1976. Die biostratigraphische Gliederung des Altpaläozoikums am Polster bei Eisenerz (Nördliche Grauwackenzone, Österreich). Verhandlungen der Geologischen Bundesanstalt, 1976, 257–303.

Frank, W., Schlager, W., 2006. Jurassic strike-slip versus subduction in the Eastern Alps. International Journal of Earth Sciences, 95, 431–450. https://doi.org/10.1007/s00531-005-0045-7

Gain, S.E.M., Greau, Y., Belousova, H. H. E., Dainis I., Griffin, W. L., O'Reilly, S. Y., 2019. Mud Tank Zircon: Long-Term Evaluation of a Reference Material for U-Pb Dating, Hf-Isotope Analysis and Trace Element Analysis. Geostandards and Geoanalytical Research 43, 339–354. https://doi.org/10.1111/ggr.12265

Grundvåg, S.-A., Jelby, M.E., Olaussen, S., Sliwinska, K.K., 2021. The role of shelf morphology on storm-bed variability and stratigraphic architecture, Lower Cretaceous, Svalbard. Sedimentology, 86, 196–237. https://doi.org/10.1111/sed.12791

Haas, I., Eichinger, S., Haller, D., Fritz, H., Nievoll, J., Mandl, M., Hippler, D., Hauzenberger, C., 2020. Gondwana fragments in the Eastern Alps: A travel story from U/Pb zircon data. Gondwana Research, 77, 204–222. https://doi.org/10.1016/j.gr.2019.07.015

Haller, D., 2016. Polyphase Deformation und Deckenstapelung in der östlichen Grauwackenzone. Master Thesis Univ. Graz, 130 pp.

Handler, R., Dallmeyer, R.D., Neubauer, F., 1997. $^{40}Ar/^{39}Ar$ ages of detrital white mica from Upper Austroalpine units in the Eastern Alps: Evidence for Cadomian and contrasting Variscan sources. Geologische Rundschau, 86, 69–80. https://doi.org/10.1007/s005310050122

Hauer, F. v., 1868. Geologische Übersichtskarte der österreichischen Monarchie. Blatt VI: Östliche Alpenländer. Jahrbuch der Geologischen Reichsanstalt, 18, 1–44.

Heinisch, H., 1980. Der ordovizische Porphyroid-Vulkanismus der Ost- und Südalpen. Diss. Univ. München, 253 pp.

Heinisch, H., 1981. Zum ordovizischen „Porphyroid"-Vulkanismus der Ost- und Südalpen, Stratigraphie, Petrographie, Geochemie. Jahrbuch der Geologischen Bundesanstalt, 124, 1–109.

Heinisch, H., Pestal, G., Reitner, J.M., 2015. Erläuterungen zu Blatt 122 Kitzbühel. Geologische Bundesanstalt, 301 pp.

Horstwood, M. S. A., Košler, J., Gehrels, G., Jackson, S. E., McLean, N. M., Paton, C., Pearson, N. J., Sircombe, K., Sylvester, P., Vermeesch, P., Bowring, J. F., Condon, D. J., Schoene, B. 2016. Community-Derived Standards for LA-ICP-MS U-(Th-)Pb Geochronology – Uncertainty Propagation, Age Interpretation and Data Reporting. Geostandards and Geoanalytical Research, 40(3), 311–332. https://doi.org/10.1111/j.1751-908X.2016.00379.x

Hubmann, B., Ebner, F., Ferretti, A., Kido, E., Krainer, K., Neubauer, F., Schönlaub, H.P., Suttner, T.J., 2014. The Paleozoic Era(them). – In: Piller, W.E. (Ed.): The lithostratigraphic units of the Austrian Stratigraphic Chart 2004 (sedimentary successions) – Vol I, Second Edition. Abhandlungen der Geologischen Bundesanstalt, 66, 9–133.

Jackson, S.E., Pearson, N.J., Griffin, W.L., Belousova, E.A., 2004. The application of laser ablation-inductively coupled plasma-mass spectrometry (LA-ICP-MS) to in-situ U–Pb zircon geochronology. Chemical Geology, 211, 47–69. https://doi.org/10.1016/j.chemgeo.2004.06.017

Jaffey, A.H., Flynn, K.F., Glendenin, L.E., Bentley, W.C., Essling, A.M. 1971. Precision Measurement of Half-Lives and Specific Activities of ^{235}U and ^{238}U. Physical Review C 4, 1889–1906. https://doi.org/10.1103/PhysRevC.4.1889

Košler, J., 2008. Laser ablation sampling strategies for concentration and isotope ratio analyses by ICP-MS. In: Sylvester, P. (Ed.), Laser Ablation ICP-MS in the Earth Sciences: Current Practices and Outstanding Issues. Mineralogical Association of Canada Short Course, 40, 79–92. Vancouver, B.C.

Le Bas, M. J., Le Maitre, R.W., Streckeisen, A., Zanettin, B., 1986. A Chemical Classification of Volcanic Rocks based on the Total Alkali-Silica Diagram. Journal of Petrology, 27, 745–750. https://doi.org/10.1093/petrology/27.3.745

Maaløe, S., Petersen, T.S., 1981. Petrogenesis of Oceanic Andesites. Journal of Geophysical Research, 86, 10273–10286. https://doi.org/10.1029/JB086iB11p10273

Mandl, G.W., 2015. Das Kalkalpine Stockwerk auf GK50 Blatt 103 Kindberg. Arbeitstagung der Geologischen Bundesanstalt, 21.-25. September 2015, Mitterdorf im Mürztal, 87 – 125.

Mandl, M., Kurz, W., Hauzenberger, C., Fritz, H., Klötzli, U., Schuster, R., 2018. Pre-Alpine evolution of the Seckau Complex (Austroalpine basement/Eastern Alps): Constraints from in-situ LA-ICP-MS U/Pb zircon geochronology. Lithos, 296–299, 412–430. https://doi.org/10.1016/j.lithos.2017.11.022

Meinhold, G., Morton, A.C., Avigad, D., 2013. New insights into peri-Gondwana paleogeography and the Gondwana super-fan system from detrital zircon U–Pb ages. Gondwana Research, 23, 661–665. https://doi.org/10.1016/j.gr.2021.05.003

Meli, S., Klötzli, U.S., 2001. Evidence for Lower Paleozoic magmatism in the Eastern South Alpine basement: zircon geochronology from the Comelico porphyroids. Schweizerische Mineralogische und Petrographische Mitteilungen, 81, 147–157. https://doi.org/10.5169/seals-61684

Metz, K., 1938. Geologie der Grauwackenzone von Leoben bis Mautern. Jahrbuch der Geologischen Bundesanstalt, 88, 165–193.

Miyashiro, A., 1974. Volcanic rock series in island arcs and active continental margins . American Journal of Science, 274, 321–355. https://doi.org/10.2475/ajs.274.4.321

Nasdala, L., Hofmeister, W., Norberg, N., Martinson, J. M., Corfu, F., Dörr, W., Kamo, S. L., Kennedy, A. K., Kronz, A., Reiners, P. W., 2008. Zircon M257 - a homogeneous natural reference material for the ion microprobe U-Pb analysis of zircon. Geostandards and Geoanalytical Research 32, 247–265. https://doi.org/10.1111/j.1751-908X.2008.00914.x

Neubauer, F., 1989. Late Variscan structures of the Eastern Greywacke Zone (Eastern Alps). Neues Jahrbuch für Geologie und Paläontologie - Monatshefte, 425–432. https://doi.org/10.1127/njgpm/1989/1989/425

Neubauer, F., Frisch, W., Hansen, B.T., 2002. Early Palaeozoic tectonothermal events in basement complexes of the eastern Greywacke Zone (Eastern Alps): evidence from U-Pb zircon data. International Journal of Earth Science, 91, 775–786. https://doi.org/10.1007/s00531-001-0254-7

Neubauer, F., Handler, R., Hermann, S., Paulus, G., 1994. Revised Lithostratigraphy and Structure of the Eastern Graywacke Zone (Eastern Alps). Mitteilungen der österreichischen geologischen Gesellschaft, 86, 61–74.

Neubauer, F., Liu, Y., Chang, R., Yuan, S., Yu, S., Genser, J., Liu, B., Guan, Q., 2020. The Wechsel Gneiss Complex of Eastern Alps: an Ediacaran to Cambrian continental arc and its Early Proterozoic hinterland. Swiss Journal of Geosciences, 113:21. https://doi.org/10.1186/s00015-020-00373-3

Neubauer, F., Vozarova, A., 1990. The Noetsch-Veitsch-North Gemeric Zone of Alps and Carpathians: Correlation, Paleogeographics and Geodynamics Significance for Variscan Orogeny. In: Minarikova, D., Lobitzer, H. (eds.): Thirty years of geological cooperation between Austria and Czechoslovakia. Ustredni Ustav Geologicky, Prague, 167–171.

Nievoll, J., 1983. Stratigraphische und strukturgeologische Untersuchungen in der Grauwackenzone bei Veitsch (Steiermark). Diss. Univ. Graz, 150 pp.

Nievoll, J., 1984. Der Südrand der Grauwackenzone zwischen Stübming und Neuberg (Obersteiermark, ÖK 103 Kindberg). Mitteilungen der österreichischen geologischen Gesellschaft, 77, 63–71.

Nievoll, J., 1987. The Lower Paleozoic of the Noric nappe at Veitsch (Eastern Alps, Austria). In: Flügel, H.W., Sassi, F.P., Grecula, P. (Eds.), Pre-Variscan and Variscan Events in the Alpine-Mediterranean Mountain Belts. Mineralia Slovaca Monography, 379–386.

Nievoll, J., 2015. Alpidische Tektonik in der Norischen Decke der östlichen Grauwackenzone zwischen Neuberg und Turnau (GK50 Blatt 103 Kindberg). Arbeitstagung der Geologischen Bundesanstalt, 21.-25. September 2015, Mitterdorf im Mürztal, 44–57.

Nievoll, J., Suttner, T.J., 2015. Stratigrafie der Norischen Decke auf GK50 Blatt 103 Kindberg. Arbeitstagung der Geologischen Bundesanstalt, 21.-25. September 2015, Mitterdorf im Mürztal, 58–69.

Paton, C., Hellstrom, J., Paul, B., Woodhead, J., Hergt, J., 2011. Iolite: Freeware for the visualisation and processing of mass spectrometric data. Journal of Analytical Atomic Spectrometry, 26, 2508–2518. https://doi.org/10.1039/c1ja10172b

Paton, C., Woodhead, J. D., Hellstrom, J. C., Hergt, J. M., Greig, A., Maas, R., 2010. Improved laser ablation U-Pb zircon geochronology through robust downhole fractionation correction. Geochemistry, Geophysics, Geosystems, 11(3). https://doi.org/10.1029/2009GC002618

Peakall, J., Best, J., Baas, J.H., Hodgson, D.M., Clare, M.A., Talling, P.J. Dorrell, R.M., Lee, D.L., 2020. An integrated process-based model of flute and tool marks in deep-water environments: Implications for palaeohydraulics, the Bouma sequence and hybrid event beds. Sedimentology, 67, 1601–1666. https://doi.org/10.1111/sed.12727

Peccerillo, A., Taylor, S.R., 1976. Geochemistry of Eocene calc-alkaline volcanic rocks from the Kastamonu area, Northern Turkey. Contributions Mineralogy and Petrology, 58, 63–81. https://doi.org/10.1007/BF00384745

Pickering, K., Stow, D., Watson, M., Hiscott, R., 1986. Deep-water facies, processes and models: a review and classification scheme for modern and ancient sediments. Earth-Science Reviews, 23, 75–174. https://doi.org/10.1016/0012-8252(86)90001-2

Rantitsch, G., Bryda, G., Gawlick, H.-J., 2020. Conodont thermometry by Raman spectroscopy on carbonaceous material: a case study from the Northern Calcareous Alps (Mürzalpen Nappe, Eastern Alps). Austrian Journal of Earth Sciences, 113, 201–210. https://doi.org/10.17738/ajes/2020.0012

Reineck, H.E., Singh, I.B., 1972. Genesis of laminated sand and graded rhytmites in storm-sand layers of shelf mud. Sedimentology, 18, 123–128. https://doi.org/10.1111/j.1365-3091.1972.tb00007.x

Ratschbacher, L., 1984. Beitrag zur Neugliederung der Veitscher Decke (Grauwackenzone) in ihrem Westabschnitt (Obersteiermark, Österreich). Jahrbuch der Geologischen Bundesanstalt, 127, 423–453.

Ratschbacher, L., 1986. Kinematics of Austro-Alpine cover nappes: changing translation path due to transpression. Tectonophysics, 125, 335–356. https://doi.org/10.1016/0040-1951(86)90170-8

Rubatto, D., 2002. Zircon trace element geochemistry: partitioning with garnet and the link between U-Pb ages and metamorphism. Chemical Geology, 184, 123–138. https://doi.org/10.1016/S0009-2541(01)00355-2

Schlaegel-Blaut, P., 1990. Der basische Magmatismus der Nördlichen Grauwackenzone, Oberostalpines Paläozoikum. Abhandlungen der Geologischen Bundesanstalt, 43, 149 pp.

Schönlaub, H.P., 2000. The Ordovician of the Southern Alps. Mitteilungen der österreichischen geologischen Gesellschaft, 91 (1998), 39–51.

Schönlaub, H.P., Flajs, G., Thalmann, F., 1980. Conodontenstratigraphie am Steirischen Erzberg (Nördliche Grauwackenzone). Jahrbuch der Geologischen Bundesanstalt, 123, 169–229.

Schönlaub, H.P., Flajs, G., 1993. Neue Fossilfunde in den westlichen Karnischen Alpen. Jahrbuch der Geologischen Bundesanstalt, 136, 233–245.

Schönlaub, H.P.,1982. Die Grauwackenzone in den Eisenerzer Alpen (Österreich). Jahrbuch der Geologischen Bundesanstalt, 124, 361–423.

Schouppe, A.v., 1854. Geognostische Bemerkungen über den Erzberg bei Eisenerz und dessen Umgebungen. Jahrbuch der Geologischen Reichsanstalt, 5, 396–406.

Schuster, R., 2015. Grauwackenzone und Grauwackenzone-Deckensystem. Arbeitstagung der Geologischen Bundesanstalt, 21.-25. September 2015, Mitterdorf im Mürztal, 38–43.

Schuster, R., Frank, W., 1999. Metamorphic evolution of the Austroalpine units east of the Tauern window: indications for Jurassic strike-slip tectonics. Mitteilungen der Gesellschaft der Geologie- und Bergbaustudenten in Österreich, 42, 37–58.

Schuster, R., Nowotny, A., 2015. Die Einheiten des Ostalpinen Kristallins auf den Kartenblättern GK50 Blatt 103 Kindberg und 135 Birkfeld. Arbeitstagung der Geologischen Bundesanstalt, 21.-25. September 2015, Mitterdorf im Mürztal, 10–37.

Shand, S.J., 1943. Eruptive rocks: their genesis, composition, classification, and their relation to ore deposits with a chaper on meteorites, Imprenta Verlag, London, 444 pp.

Sláma, J., Košler, J., Condon, D.J., Crowley, J.L., Gerdes, A., Hanchar, J.M., Horstwood, M.S.W., Morris, G.A., Nasdala, L., Norberg, N., Schaltegger, U., Schoene, B., Tubrett, M.N., Whitehouse, M.J., 2008. Plešovice zircon – a new natural reference material for U/Pb and Hf isotopic microanalysis. Chemical Geology, 249, 1–35. https://doi.org/10.1016/j.chemgeo.2007.11.005

Söllner, F., Höll, R., Miller, H., 1991. U-Pb-Systematik der Zirkone in Metavulkaniten („Porphyroiden") aus der Nördlichen Grauwackenzone und dem Tauernfenster (Ostalpen, Österreich). Zeitschrift der Deutschen Geologischen Gesellschaft, 142, 285–299. https://doi.org/10.1127/zdgg/142/1991/285

Söllner, F., Miller, H., Höll, R., 1997. Alter und Genese rhyodazitischer Metavulkanite („Porphyroide") aus der Nördlichen Grauwackenzone und der Karnischen Alpen (Österreich): Ergebnisse von U-Pb-Zirkondatierungen. Zeitschrift der Deutschen Geologischen Gesellschaft, 148, 499–522. https://doi.org/10.1127/zdgg/148/1997/499

Spychala, Y.T., Eggenhuisen, J.T., Tilston, M., Pohl, F., 2020. The influence of basin setting and turbidity current properties on the dimensions of submarine lobe elements. Sedimentology, 67, 3471–3491. https://doi.org/10.1111/sed.12751

Spychala, Y.T., Hodgson, D.M., Prélat, A., Kane, I.A., Flint, S.S., Mountney, N.P., 2017. Frontal and lateral submarine lobe fringes: Comparing sedimentary facies, architecture and flow processes. Journal of Sedimentary Research, 87, 75–96. http://dx.doi.org/10.2110/jsr.2017.2

Stur, D., 1865. Vorkommen ober-silurischer Petrefacte am Erzberg und in dessen Umgebung. Jahrbuch der Geologischen Reichsanstalt, 15, 267–277.

Stur, D., 1871. Geologie der Steiermark. 654 pp., Graz.

Tinterri, R., Muzzi Magalhaes, P., Tagliaferri, A., Cunha, R.S., 2016. Convolute laminations and load structures in turbidites as indicators of flow reflections and decelerations against bounding slopes. Examples from the Marnoso-arenacea Formation (northern Italy) and Annot Sandstones (south eastern France). Sedimentary Geology, 344, 382–407. https://doi.org/10.1016/j.sedgeo.2016.01.023

Vermeesch, P., 2018. IsoplotR: A free and open toolbox for geochronology. Geoscience Frontiers, 9, 1479–1493. https://doi.org/10.1016/j.gsf.2018.04.001

Vermeesch, P., 2012. On the visualisation of detrital age distributions. Chemical Geology, 312-313, 190–194. https://doi.org/10.1016/j.chemgeo.2012.04.021

Watson, E.B., Harrison, T.M., 1983. Zircon saturation revisited: temperature and composition effects in a variety of crustal magma types. Earth and Planetary Science Letters, 64, 295–304. https://doi.org/10.1016/0012-821X(83)90211-X

Wiedenbeck, M.A.P.C., Alle, P., Corfu, F., Griffin, W. L., Meier, M., Oberli, F. V., Quadt, A. V., Roddick, J. C., Spiegel, W., 1995. Three natural zircon standards for U-Th-Pb, Lu-Hf, trace element and REE analyses. Geostandards Newsletter 19, 1–23. https://doi.org/10.1111/j.1751-908X.1995.tb00147.x

Wu, J., Cronin, S.J., Rowe, M.C., Wolff, J.A., Barker, S.J., Fu, B., Boroughs, S., 2021. Crustal evolution leading to successive rhyolitic supereruptions in the Jemez Mountains volcanic field, New Mexico, USA. Lithos, 396–397. https://doi.org/10.1016/j.lithos.2021.106201

Zurbriggen, R., 2017. The Cenerian orogeny (early Paleozoic) from the perspective of the Alpine region. International Journal of Earth Sciences, 106, 517–529. https://dx.doi.org/10.1007/s00531-017-1496-3

Received: 12.9.2021
Accepted: 5.2.2022
Editorial Handling: Hugo Ortner

Appendix

Analytical conditions for LA-ICP-MS zircon analyses.

Laboratory name: NAWI Graz Central Lab for Water, Minerals and Rocks (University of Graz and Graz University of Technology). Sample type and preparation: Zircon; Conventional mineral separation. Single grains embedded in 1 inch resin mount. Final polishing with 1 µm diamond paste.
Imaging: JXA-8530F Plus HyperProbe (BSE and CL). Analytical session(s): 20-21/11/2017 (samples WASCH, A1, A4); 23/01/2020 - 19/02/2020; (samples S1, S2, S3, S4); 22/02/2021 (samples BGR2, MGR3, MGR4, SOE2, S36).

Laser Ablation System:
Instrument: NWR193 ArF Excimer laser (ESI, Portland. U.S.A.)
Cell type: Two volume ablation cell
Laser wavelength: 193 nm
Pulse duration: 4-6 ns
Fluence: ~ 2.5-2.7 J/cm2
Sampling mode: Line scan with line scan, length 50-150 µm, scan speed 10 µm/s (samples WASCH, A1, A4). Single hole drilling, circular shape.
Pre-ablation cleaning: 1 burst 20 µm
Spot diameter (nominal): 35 µm, 15 µm (spot data); 10-15 µm (line scan)
Repetition rate: 5 Hz (spot); 7-10 Hz (line scan).
Ablation duration: 15 s (spot); 100 s (line scan).
Carrier gas: He gas (combined with Ar outside the ablation cell).
He gas flow rate: 0.75 L/min.
Ar mix gas flow rate: 0.75 L/min

ICP Mass Spectrometer:
Instrument: Nu PlasmaII HR-MC-ICP-MS (Nu Instruments, Wrexham, U.K.).
Sample introduction: Ablation aerosol only.
RF power: 1300 W.
Monitored masses: ^{202}Hg, ^{204}(Hg + Pb), ^{206}Pb, ^{207}Pb, 208Pb, ^{232}Th, ^{238}U
Detectors: 5 electron-multiplier, ion-counting detectors (IC) and 2 Faraday collectors (H): IC4 for ^{202}Hg, IC3 for ^{204}(Hg + Pb), IC2 for ^{206}Pb, IC1 for ^{207}Pb, IC0 for ^{208}Pb, H7 for ^{232}Th, H9 for ^{238}U.
Tuning: Line scan on NIST SRM 612 glass to optimize sensitivity and peak shapes for all monitored masses.
Analysis mode: Time Resolved Analysis.
Integration time for single data point: 0,2 s (spot), 1 s (line scan)

Data processing:
Mass discrimination: Instrumental mass bias corrected by bracketing of unknown samples with primary reference material for isotope ratios and element concentrations.
Data reduction: For Spot: U-Pb zircon geochronology Data Reduction Scheme (U_PbGeochron4) for Iolite 3.71 (Paton et al., 2010; 2011). Blank and signal integrations imported using laser log file. Blank windows selected between 25 and 3 s before signal, Signal windows trimmed for ~1-2 s (start) and ~2 s (end).
For line scan: MS Excel spreadsheet LamTool U-Th-Pb version VI (Košler, 2008).
Gas blank: For Spot: Gas blank (25 seconds) acquired before each analysis and subtracted with step-forward method. For line scan: Gas blank (30-35 seconds) acquired before each analysis.
Primary reference material: For spot data: GJ-1 zircon (Jackson et al., 2004). For line scan: Plesovice zircon (Sláma et al., 2008).
Normalization values: ^{206}Pb/^{238}U = 0.097860, ^{207}Pb/^{235}U = 0.81117, ^{208}Pb/^{232}Th = 0.03074, ^{207}Pb/^{206}Pb = 0.060139 (Horstwood et al., 2016); U content = 342 ppm, Th content = 9.7 ppm, Pb content = 30 ppm.
Decay constants of Jaffey et al. (1971); Common-Pb correction: None.
Uncertainties: Single spot: Internal uncertainty and propagated excess scatter from primary standard analyses (2SE). Weighted mean results: weighted mean uncertainty and long-term variance of validation material (1.3%) added by quadratic addition (2SD).
Secondary reference material for quality check: Line Scan: Plesovice zircon (^{206}Pb/^{238}U age = 337.13±0.37 Ma, ID-TIMS; Sláma et al., 2008); 91500 zircon (^{206}Pb/^{238}U age = 1063.51 Ma, ID-TIMS; Horstwood et al., 2016); M257 (^{206}Pb/^{238}U age = 1, ID-TIMS; Nasdala et al., 2008); Mud Tank zircon (Concordia age 731±0.2 Ma; Black and Gulson, 1978; Gain et al., 2019).
Secondary reference material results: For spot data: Plesovice: Weighted mean ^{206}Pb/^{238}U age = 337.2 ± 4.6 Ma (2 SD, MSWD = 2.3, n = 50, in 3 sessions). 91500: Weighted mean ^{206}Pb/^{238}U age = 1074 ± 14.7 Ma (2 SD, MSWD = 2.4, n = 43, in 3 sessions). For line scans: Plesovice: Weighted mean ^{206}Pb/^{238}U age = 337.6 ± 2.4 Ma (2 SD, MSWD = 2.4, n = 90, in 3 sessions). 91500: Weighted mean ^{206}Pb/^{238}U age = 1064.2 ± 2,0 Ma (2 SD, MSWD = 2.0, n = 44, in 3 sessions). Mud Tank: Weighted mean ^{206}Pb/^{238}U age = 730.9 ± 2.0 Ma (2 SD, MSWD = 0.8, n = 46, in 2 sessions).

Name-giving locations			
Formation Name	East	North	Location
Rad Fm.	15.439	47.621	Wirtshaus zu Radwirt
Stocker Fm.	15.445	47.630	Stocker Hill
Sommerauer Fm.	15.355	47.654	Sommerauer Homestead
Kaskögerl Fm.	15.481	47.636	Kaskögerl Mountain
Kaiserstein Fm.	15.381	47.622	Kaiserstein Mountain
Geochronology samples			
Sample Nr.	East	North	Unit / Rock-Type
WASCH	15.513	47.618	Creek sediment
BGR2	15.343	47.581	Blasseneck Porphyroid
MGR3	15.547	47.627	Blasseneck Porphyroid
MGR4	15.548	47.627	Blasseneck Porphyroid
SOE2	15.332	47.663	Blasseneck Porphyroid
S2	15.474	47.639	Stocker Fm. Volcanics
S36	15.474	47.640	Stocker Fm. Volcanics
S1	15.473	47.636	Stocker Fm. Sandstone
S4	15.444	47.624	Stocker Fm. Sandstone
S36	15.474	47.640	Stocker Fm. Sandstone
A1	15.363	47.650	Sommerauer Fm. Sandstone
A4	15.352	47.648	Sommerauer Fm. Sandstone
Geochemistry samples			
Sample Nr.	East	North	Unit / Rock-Type
BGR1	15.343	47.577	Blasseneck Porphyroid
BGR2	15.343	47.581	Blasseneck Porphyroid
SOE1	15.332	47.664	Blasseneck Porphyroid
SOE2	15.332	47.663	Blasseneck Porphyroid
MGR02	15.532	47.613	Blasseneck Porphyroid
MGR03	15.547	47.627	Blasseneck Porphyroid
MGR10	15.547	47.627	Blasseneck Porphyroid
MGR04	15.548	47.627	Blasseneck Porphyroid
K6	15.488	46.643	Stocker Fm. Volcanics
K8	15.488	46.643	Stocker Fm. Volcanics
S2	15.474	47.639	Stocker Fm. Volcanics
S33	15.474	47.635	Stocker Fm. Volcanics
S81b	15.464	47.635	Stocker Fm. Volcanics
S24	15.442	47.627	Stocker Fm. Volcanics
S80/3	15.426	47.622	Stocker Fm. Volcanics
S25a	15.443	47.630	Stocker Fm. Volcanics
S25b	15.443	47.630	Stocker Fm. Volcanics
S98	15.351	47.610	Stocker Fm. Volcanics
S103	15.360	47.612	Stocker Fm. Volcanics

Table A1: Geographic coordinates of samples in decimal degrees.

Major elements (wt %)

Sample	Rock	SiO_2	TiO_2	Al_2O_3	Fe_2O_3	MnO	MgO	CaO	K_2O	Na_2O	P_2O_5	LOI	Sum
BGR1	BP	69.69675	0.33	14.91	3.02	0.037	1.32	2.8	1.9	3.35	0.096	1.36	98.82
BGR2	BP	62.72205	0.66	16.56	5.23	0.066	1.9	3.48	3.18	3.13	0.19	1.93	99.05
SOE1	BP	68.4405	0.35	14.55	4.01	0.027	3.18	1.41	2.64	1.54	0.078	2.81	99.04
SOE2	BP	75.20415	0.29	13.01	2.43	0.008	0.64	0.03	4.1	1.63	0.069	1.84	99.25
MGR2	BP	68.67165	0.43	15.01	3.72	0.042	2.13	2.21	2.27	2.73	0.103	1.83	99.15
MGR2	BP	63.70695	0.54	15.54	5.16	0.032	5.65	0.49	3.47	0.66	0.154	4.04	99.44
MGR1	BP	72.7017	0.23	14.03	2.51	0.061	1.82	0.27	3.16	2.28	0.047	1.93	99.04
MGG4	BP	75.4755	0.13	13.23	1.63	0.038	0.71	1.14	2.1	3.97	0.029	1.11	99.56
K6	MV	74.5509	0.13	13.95	1.49	0.029	0.75	0.05	2.9	3.28	0.03	1.73	98.89
K8	MV	74.4705	0.12	14.25	1.43	0.022	0.73	0	2.39	3.91	0.03	1.32	98.67
S2	MV	57.5463	0.54	14.61	5.73	0.114	5.76	2.93	0.5	4.88	0.125	6.61	99.35
S33	MV	57.3	0.51	14.39	5.42	0.11	6.54	3.18	0.34	5.42	0.13	6.98	100.32
S81b	MV	71.98	0.18	15.32	1.82	0.01	2.06	0.02	2.43	4.32	0.04	1.83	100.01
S24	MV	83.3	0.14	7.08	1.73	0.02	4.29	0.07	1.1	1.45	0.05	na	99.23
S80/3	MV	82.2	0.04	10.1	0.47	0	1.9	0.02	1.42	3.7	0.02	na	99.87
S25a	MV	71.97	0.31	14.94	3.52	0.04	1.86	0.09	2.76	2.18	0.06	2.40	100.13
S25b	MV	73.55	0.29	14.9	2.34	0.11	1.13	0.36	2.56	2.86	0.06	1.83	99.99
S98	MV	79.1	0.18	12.4	2.37	0.01	1.49	0.01	2.26	2.08	0.01	na	99.91
S103	MV	77.6	0.18	13.59	2.61	0.01	1.77	0.01	2.58	1.6	0.01	na	99.96
V 1	BP	69.37	0.69	14.78	4.66	0.05	2.61	2.71	2.24	1.97	0.30	2.42	99.38
V 2	BP	67.81	0.49	15.83	4.06	0.09	1.43	2.21	2.55	5.28	0.28	1.75	100.03
V 3	BP	67.14	0.53	15.69	4.51	0.09	1.93	2.87	3.17	3.45	0.38	3.20	99.76
V 4	BP	67.02	0.53	16.66	4.68	0.06	2.94	1.36	2.95	3.46	0.13	3.30	99.79
V 5	BP	67.04	0.54	16.28	4.82	0.07	2.62	1.51	2.49	4.19	0.18	2.95	99.74
V 6	BP	71.06	0.39	15.45	3.35	0.04	1.55	1.17	2.53	4.10	0.10	2.26	99.74
V 7	BP	67.98	0.6	14.88	4.68	0.06	1.52	2.34	4.14	2.88	0.21	3.49	99.29
V 8	BP	66.99	0.6	15.77	4.30	0.10	1.51	2.02	3.76	3.85	0.27	3.07	99.17
V 9	BP	69.38	0.46	15.75	3.09	0.08	1.39	1.74	4.41	3.18	0.22	2.43	99.70
V 10	BP	68.74	0.51	15.33	3.70	0.05	1.46	2.40	3.58	3.30	0.23	2.19	99.30
V 11	BP	63.58	0.88	16.38	5.48	0.09	3.03	5.94	2.16	1.64	0.47	2.65	99.65
V 12	BP	67.85	0.54	15.88	4.69	0.07	1.71	1.06	3.38	4.17	0.18	1.90	99.53
V 13	BP	67.03	0.6	15.5	4.91	0.08	2.60	2.41	2.94	3.27	0.25	3.50	99.59
V 14	BP	66.88	0.61	15.86	4.11	0.05	1.90	3.38	3.05	3.75	0.26	4.49	99.85
V 15	BP	64.36	0.62	18.61	5.00	0.06	1.97	1.55	3.87	3.31	0.30	2.93	99.65
V 16	BP	68.39	0.56	14.79	3.91	0.09	2.06	2.61	3.56	3.69	0.24	3.69	99.90
V 17	BP	66.74	0.63	15.38	4.70	0.10	2.05	3.52	2.97	3.23	0.28	3.03	99.60

Selected Trace elements (ppm)

Sample	V	Cr	Ni	Cu	Zn	Ga	Rb	Sr	Y	Zr	Ba	Ce	Nd	Pb	Zr
BGR1	43.1	<20	<20	<20	39.7	18.6	55.7	547.9	29.2	148	603.6	66.5	22.4	<20	148
BGR2	91.9	51.9	<20	<20	67.2	20	107.7	366.5	31.5	210.6	971.2	93.8	36.5	<20	210.6
SOE1	39	<20	<20	<20	58.1	16.6	78.3	170.6	31.6	165.1	502.9	55.5	33.3	<20	165.1
SOE2	30.9	<20	<20	<20	18.3	15.3	162.4	12.2	34	140.1	209.1	84.2	35.3	<20	140.1
MGR2	48.7	<20	<20	<20	70.6	19.6	87.2	135.8	30.6	170	763	86.2	22.7	<20	170
MGR3	72.7	35.5	25.4	<20	31.1	19	130.2	17.8	14.1	187.5	790.3	31.1	<20	<20	187.5
MGR1	26.8	<20	<20	<20	44.5	17.2	121.1	48.1	20.1	152.6	649.3	104	20.6	<20	152.6
MGR4	<20	<20	<20	<20	31.2	16.5	83.9	73	32.4	97.6	440	30.2	22.2	21.5	97.6
K6	<20	<20	<20	<20	20.6	21.9	136.4	25.3	47.1	159.7	979	121.7	37.9	<20	159.7
K8	<20	<20	<20	<20	24.2	19.7	107.8	28.8	46.7	147	505.3	65.9	20.9	<20	147
S2	121.8	197.7	97.2	<20	55.3	16.2	27.1	186.9	19.1	115.5	195.2	65.6	<20	<20	115.5
V 1	62	34	32	24	54	20	97	393	40	284	na	na	na	24	284
V 2	47	19	31	23	47	21	123	345	45	276	na	na	na	24	276
V 3	93	1	29	16	262	21	111	428	40	273	na	na	na	23	273
V 4	79	28	29	10	51	21	120	93	42	229	na	na	na	17	229
V 5	76	45	43	24	49	21	107	148	42	255	na	na	na	19	255
V 6	73	1	38	26	45	22	126	120	46	255	na	na	na	28	255
V 7	54	34	27	32	34	23	165	165	45	253	na	na	na	38	253
V 8	17	29	18	22	44	20	107	107	49	268	na	na	na	20	268
V 9	58	1	15	19	42	20	177	177	53	277	na	na	na	24	277
V 10	52	3	14	15	43	21	372	372	50	301	na	na	na	32	301
V 11	63	80	34	15	49	21	932	932	43	374	na	na	na	35	374
V 12	126	37	24	9	15	18	159	159	45	241	na	na	na	17	241
V 13	55	19	16	22	54	21	162	162	45	262	na	na	na	23	262
V 14	18	77	28	23	44	21	620	620	48	354	na	na	na	24	354
V 15	35	54	17	20	51	22	102	102	50	272	na	na	na	21	272
V 16	74	19	18	21	35	19	152	162	48	258	na	na	na	23	258
V 17	54	73	25	11	48	19	340	340	46	287	na	na	na	17	287

Table A2: Major and trace element compositions of samples from Blassneneck Porphyroids (BP) and metavolcanics of the Stocker Formation (MV). V are Blasseneck Porphyroids analyzed by Heinisch (1980), samples S33, S81b, S24, S80/3, S25a, S25b, S98, S103 were analyzed at the Quality Management Department of RHI Magnesita´s Veitsch plant. All other samples at Institute for Earth Sciences, University of Graz.